# Electronic Properties of a Monolayer−Electrolyte Interface Obtained from Mechanistic Impedance Analysis

**Chaitanya Gupta,[†] Mark A. Shannon,*[,†,‡,§] and Paul J. A. Kenis*[,†,‡,§]**

*Departments of Chemical & Biomolecular Engineering and Mechanical Science & Engineering and Beckman Institute for Advanced Science and Technology, University of Illinois at Urbana−Champaign, Urbana, IL-61801*

*Received: January 31, 2009; Revised Manuscript Received: April 7, 2009*

We report here a methodology to measure and characterize the interface properties of thin, insulating films that separate a gold electrode and an electrolyte solution, for cases when the electrolyte solution does not contain electro-active ions in appreciable amounts, by using experimental impedance data. Traditionally, in the absence of redox-active species either in the electrolyte or at the terminal headgroup, monolayer films on polycrystalline gold electrodes have been modeled as ideal dielectric capacitors. However, potential-dependent background currents are usually observed for gold−monolayer−electrolyte systems, even in the absence of redox-active moieties. A qualitative description of the background current density as a barrier-limited flux of charge that applies irrespective of the actual mechanism of charge transport through the monolayer film is proposed in this paper. The potential-dependent, low-frequency impedance data is shown to characterize the properties of this limiting energy barrier. On the basis of this description for the flow of charge through a gold−monolayer−electrolyte system, we modified the equation for charge transport to yield a constitutive expression for the low-frequency admittance of the gold−monolayer−electrolyte system. The derived expression is equally applicable to charge transport via electronic currents through the monolayer phase or by ion migration through pinhole defects in the monolayer film. The mobility and diffusivity of charge carriers within the monolayer film are unknown parameters in the equation for the system admittance. An approach that enables the estimation of these transport parameters is outlined. A comparison of the calculated mobility with published data reveals that electron transport through the monolayer phase, and not ion penetration through pinhole defects, is the dominant mechanism for charge transport. We fit the derived admittance equation containing these estimated transport parameters to the experimentally determined low-frequency admittance to provide a quantitative description of the electronic properties of the monolayer−electrolyte interface in terms of two related physicochemical properties: (a) the equilibrium chemical potential difference between the metal and the monolayer−electrolyte interface and (b) the residual or built-in electric field within the monolayer. These two properties characterize the monolayer−electrolyte interface within a specific potential regime where the current density is shown to be limited by the kinetics of electron transport through the monolayer. We also demonstrate a qualitative analogy between the gold−monolayer−electrolyte system and a Mott−Schottky rectifying barrier, on the basis of our description of the monolayer−electrolyte interface in terms of these two properties, that helps explain the anisotropic current−voltage characteristics of the monolayer-on-gold system. The effects of varying electrolyte pH, monolayer film thickness and terminal headgroup on the two physicochemical properties are also analyzed here.



## Introduction

A self-assembled monolayer (SAM) is an organized structure of surfactant molecules that adsorb at a solid−liquid interface and form well-ordered assemblies on the surface of the solid.[1−3] These organic molecules form semicrystalline, ultrathin, homogeneous films with reproducible electronic properties that can modify the interfacial properties of the solid in a controllable manner.[4] Thus, solid electrode surfaces modified by these SAMs have been used extensively as platforms to investigate the effects of monolayer thickness and functional end groups on electron transfer.[5−10] Electron transfer for $\omega$-functionalized monolayers adsorbed on gold has been extensively studied for cases when an electron donating/accepting redox-active species is dissolved in the electrolyte[11−13] as well as for situations when a redox-active species is tethered to the alkyl chain.[5,7,14−18] Different electrochemical tools such as chronoamperometry,[19] cyclic voltammetry,[5,13,19,20] and coulostatic capacitance measurements,[9] have been used extensively to demonstrate that the electron exchange process strongly depends on the properties of the monolayer−electrolyte interface. The effect of the interface properties on the charge transfer process is inferred (i) from the repulsive or attractive Coulombic field exerted by the functional group on dissolved electroactive species[13] or (ii) from the steric and solvation effects on the tethered redox species at the inner Helmholtz plane.[5,19,21] The underlying redox reaction occurs via a nonadiabatic interaction between the electronic orbitals of the metal phase and the vibronic continuum of the redox species, as mediated by an alkane linker. Since the alkane-functional group bonding orbitals constitute the first subunit of that linker, a strong influence of the monolayer−electrolyte

* Corresponding authors. E-mails: mshannon@uiuc.edu, kenis@uiuc.edu.
[†] Department of Chemical & Biomolecular Engineering.
[‡] Department of Mechanical Science & Engineering.
[§] Beckman Institute for Advanced Science and Technology.

10.1021/jp900918u CCC: $40.75 
Published on Web 04/29/2009

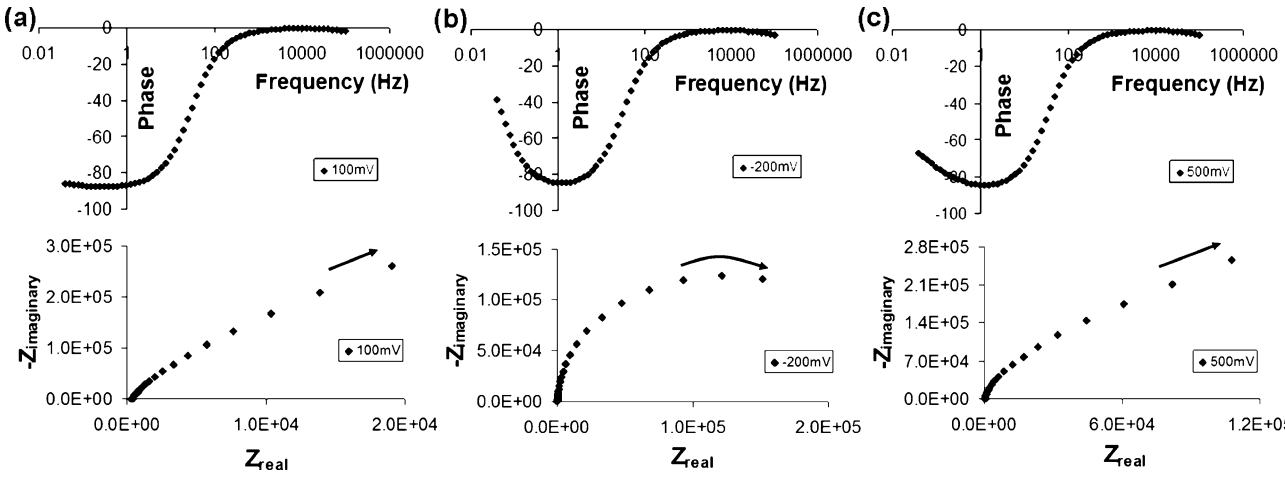


**Figure 1.** The impedance spectrum of a gold−monolayer−electrolyte system at (a) 100, (b) −200, and (c) 500 mV as seen in the Bode phase (top figure) and Nyquist (bottom figure) plots. A self-assembled monolayer film of 1-octadecane thiol on gold is the working electrode placed in a 10 mM phosphate buffer solution maintained at pH 8. Arrows in Nyquist plots indicate direction of decreasing frequency.

interface on the reaction kinetics is expected.[18,22] Therefore, a measurement of the redox charge flow can, in principle, provide a quantitative measure of the surface properties of a thin-film, modified electrode. The investigation of electron transfer in these cases, however, is limited to the use of a tethered or dissolved redox-active species that interacts with the electronic orbitals of the metal. Since the reaction kinetics are dominated by the electronic and vibrational levels of the electroactive species, background electrolyte properties such as pH and anion type do not play a significant role in the kinetics of the charge transfer process. The effect of varying the electrolyte pH is, instead, restricted to a shift in the reaction equilibrium point, as manifested by a shift in the formal potential for the electroactive species.[8] Thus, gold−monolayer−electrolyte systems in which redox-active moieties act as donor/acceptor species for the electron exchange process serve as idealized platforms for the investigation of charge transfer at and the surface characteristics of solid−liquid interfaces.

Thiol monolayers on gold are used extensively to create solid−liquid interfaces with controllable chemistries for modifying of wetting behavior,[23,24] adhesion,[25] and electrokinetic flows[26] in electrophoresis and other microfluidic devices. In a majority of these applications, there is no appreciable presence of electroactive species that act as electron donors or acceptors, either in the solution or at the inner Helmholtz plane. The effect of applying an electric potential on the surface charge density of gold−thiol monolayer nanostructures, with and without redox-active moieties, has been investigated theoretically, but most of this analysis was restricted to the ideal case of the monolayer film acting as a perfect capacitor with no net current flowing through the gold−monolayer−electrolyte system.[27−29] However, a small current density has been experimentally observed in these systems, and this flow of charge has been characterized as background or "leakage" current in literature.[30−32] Moreover, the surface chemistry at the monolayer−electrolyte interface can have a strong influence on this leakage current, as will be demonstrated in this paper as well as elsewhere.[33] The presence of a leakage current in these electrochemical gold−monolayer−electrolyte systems indicates that charge carriers such as electrons cross the solid−liquid interface under the application of an electric field, and though redox-active species are not added to the electrolyte in significant amounts, there must be ionic/neutral constituents of the electrolyte that can accept electrons from or donate electrons to the Fermi level of the gold electrode. The precise identity of these ionic or neutral species is at present unknown, and the inability to formulate a reasonable kinetic description of the charge transfer at the solid−liquid interface presents a formidable obstacle to the understanding of charge transfer in the absence of electroactive species. However, we expect that the process of electron transfer in these electrochemical systems can be described within the general framework of nonadiabatic charge transfer theory. Consequently, the current−overpotential characteristics of these thin-film systems are dominated by the vibronic−electronic interaction between the ionic/neutral electrolyte constituents and the gold. Therefore, the nature of the electrolyte has a significant effect on the leakage current and, thus, the measured surface characteristics of these thin-film-modified surfaces. To our knowledge, a quantitative description of the measurement of surface properties for monolayer films for the case in which the electrolyte does not contain electroactive species when charge flows through the monolayer film is still lacking. A comprehensive methodology that can extract surface properties from current−potential curves for a thin-film modified electrode in the absence of redox-active ions also has potential for use in sensing applications.

Electrochemical impedance spectroscopy (EIS) has proven to be a useful tool for the investigation of charge transfer at monolayer−electrolyte interfaces, especially for cases when the electrolyte may[34−37] or may not[30−32,38,39] contain a redox-active ion, since a single measurement yields information about charge transport and storage characteristics of thin-film structures as a function of time. The data is usually analyzed by fitting an equivalent circuit consisting of linear circuit elements such as resistors and capacitors to the observed frequency spectrum of the system's impedance.[10] For the case when the electrolyte has no electro-active ions, the description of a gold−monolayer−electrolyte system under the application of variable DC bias is complicated by the existence of three regimes that are defined by the magnitude of the applied potential with respect to the bulk electrolyte solution: (a) a nearly purely capacitive regime at anodic potentials (Figure 1a), in which the observed phase angle of the response is observed to be 88° (nearly 90° for pure capacitance); (b) a resistive plus capacitive regime for cathodic potentials (Figure 1b), in which the response begins to manifest predominantly real characteristics at low frequencies;[31,38] and (c) a capacitive regime at large anodic potentials (Figure 1c), in which the impedance undergoes a small but

statistically significant shift toward a more resistive response. The terms "anodic" and "cathodic" as applied to potentials describe different regimes of applied potential where the observed current density is oxidizing and reducing, respectively. The monolayer film on the polycrystalline gold electrode is known to be electrochemically stable in the potential range −500 to 500 mV, where the above-mentioned impedance responses were recorded. As discussed before, the slight deviation of the phase response of the purely capacitive regime from 90° is hypothesized to be due to leakage current, caused by substrate roughness, pinhole defects in the film, or both that facilitate ion penetration into the monolayer structure.[31,32,38] This deviation from ideality is explained by the use of the constant phase circuit element, in which the empirical shape parameter α captures the average effect of the inhomogeneties.[30] The transition between regimes (a) and (b) is said to occur due to a change in the structure of the monolayer that facilitates ion penetration, and the transition point is characterized by a threshold potential, $V_c$, that is a function of the end group in the monolayer film and the thickness of the film.[32] A subsequent paper by Burgess et al.[39] attributed the transitional behavior of monolayer films terminated by an acidic headgroup to protonation/deprotonation events occurring at the inner Helmholtz plane. We could not find a reference to the third potential regime (c) in the literature. The impedance spectrum also does not display any Warburg-like characteristics, indicating that the charge exchanging ionic/neutral electrolyte constituent is never mass-transfer-limited for any value of applied potential within the potential range.[5−10] The absence of mass transfer limitations on the impedance spectrum tends to disprove the possibility that some trace electroactive impurity in the electrolyte acts as the electron donor/acceptor. The application of a phenomenological circuit model to describe the nonlinear potential response of a gold−monolayer−electrolyte system necessitates that each regime be discussed independently of the other because no single equivalent circuit with linear components is capable of modeling the entire spectrum of impedance responses exhibited by the monolayer-modified gold electrode. Therefore, the use of equivalent circuits does not provide a mechanism that facilitates the transition of the system from one potential regime to another. The prevailing hypothesis is that the increase in current at cathodic potentials is due to electric-field-induced structural defects in the monolayer film, analogous to pores in lipid bilayer structures that permit ion flow through the membrane.[31] However, this hypothesis remains experimentally unproven. A mechanistic description for the diverse regimes that does not rely on empirical circuit models, *and which can be experimentally verified using current−potential observables*, is needed for a more complete understanding of charge transfer through monolayer modified electrode systems in the absence of redox-active moieties.

In this paper, we propose a mechanistic description of the observed current density as a flux of charge through the gold−monolayer−electrolyte system, limited by the largest of several energy barriers that can inhibit the transfer of charge from the metal to the electrolyte phase or vice versa. On the basis of this description of current density, in this paper, we introduce a comprehensive hypothesis in which an expression for the low frequency admittance of a gold−monolayer−electrolyte system is derived, which is equally applicable to charge transport via ion penetration through pinhole defects in the monolayer film or via electron migration through the alkane chains of the monolayer phase. The transport parameters in this expression (namely, the charge mobility and the charge diffusivity in the monolayer film) are estimated using a nondimensional scaling analysis. The charge mobility thus obtained indicates that electron transport through the alkane phase is the dominant mechanism of charge transport through the monolayer film. By fitting the constitutive admittance expression to experimentally observed admittance values, we demonstrate that the gold−monolayer−electrolyte systems display anisotropic current−potential behavior around a specific potential called the potential of zero field (PZF), qualitatively analogous to a solid-state Schottky barrier. Our results also demonstrate that the nature of the energy barrier limiting the charge flux is a function of the applied potential, and either charge transport through the monolayer phase or charge transfer at the monolayer−electrolyte interface is rate-limiting, depending on the potential regime. Furthermore, we determine two key physiochemical characteristics of the system (the built-in electric field within the monolayer and the equilibrium chemical potential difference of a charge carrier between the metal and the inner Helmholtz plane) that together characterize the electronic properties of the monolayer−electrolyte interface. The built-in field and the equilibrium chemical potential difference are obtained from the admittance data without appealing to a specific mechanism of charge flux through the gold−monolayer−electrolyte system. Systematic variation of these two physicochemical properties through the variation of electrolyte pH and concentration supports our hypothesis that electron transport through the alkane phase of a self-assembled monolayer, and not ion penetration through pinhole defects, is the primary mechanism of charge transport through a well-formed gold−monolayer−electrolyte system. The description of the electronic properties of the interface between a monolayer-modified gold electrode and an electrolyte solution without redox-active species also does not rely on an explicit description of the electrolyte species participating in the electron transfer reaction at the monolayer−electrolyte interface when the admittance methodology described above is used. The ionic/neutral species involved in the charge transfer process at the monolayer−electrolyte interface are described elsewhere.[33]

## Theory

**Description of Gold−Monolayer−Electrolyte System.** The estimation of physicochemical properties, characterizing the interface of a gold−monolayer−electrolyte system, from low frequency impedance data is independent of the mechanism by which charge leaks through the system, as we demonstrate in the Results and Discussion section. However, the physical significance of these properties depends on the dominant charge transport mechanism that is responsible for the flow of charge through the gold−monolayer−electrolyte system. Therefore, interpretation of the results presented in this paper requires an analysis of the various mechanisms of charge transport within the gold−monolayer−electrolyte system. Two alternate mechanisms for the "leakage current" through the monolayer film are proposed in this section: (1) the transport of charge carriers across the alkane backbone of the monolayer phase; and (2) penetration of charge carriers through pinhole defects in the monolayer film. The term "charge carriers" here refers to both electronic and ionic charge. These descriptions of charge flow are examined in the context of two different experimental systems; that is, the case of an ideal, defect-free monolayer film and the case that the monolayer film is nonideal and has large pinhole defects. The two gold−monolayer−electrolyte systems with and without large pinhole defects are also represented as in terms of their respective equivalent circuits to highlight the

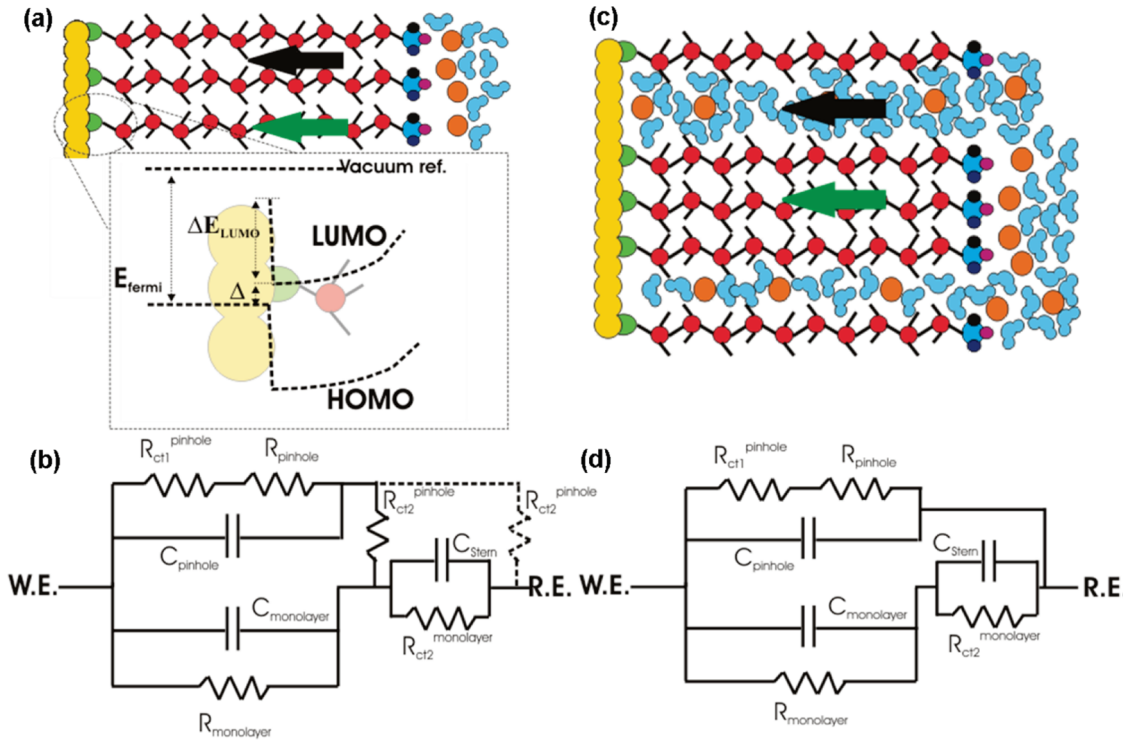


**Figure 2.** Schematic illustrating the two types of pinhole structures for an alkanethiol monolayer film that self-assembles on gold and their respective circuit diagram representations. The alkane phase that is denoted by the ball and stick model (red) chemisorbs on the gold surface (yellow) via the thiol moiety (green). The monolayer is in contact with the adjacent electrolyte phase that consists of ions (orange) solvated by the aqueous dielectric medium (sky blue). The arrows represent different charge transport mechanisms through the monolayer phase: charge carrier penetration through pinhole structure (black) and charge carrier transport through the alkane phase of monolayer film (green). The abbreviations W.E. and R.E. in the circuit diagram refer to the working and reference electrodes, respectively. For convenience, the resistance and capacitance of the accompanying diffuse layer is ignored in the circuit representation. (a) Contiguous monolayer films on smooth gold surfaces do not allow charge carrier penetration, and the Stern layer at the monolayer−electrolyte interface forms a continuous boundary between the monolayer and electrolyte phases. The expected configuration of the electronic energy levels at the gold−thiol interface is also depicted in the inset. The energy gap between the Fermi energy level of the gold substrate and the LUMO of the bulk alkane phase is assumed to be negligible. (b) Charge transfer through the gold−thiol site involves charge transfer at the monolayer−electrolyte interface ($R_{ct2}^{monolayer}$) and charge transport within the monolayer ($R_{monolayer}$). The corresponding circuit components $R_{ct2}^{pinhole}$, $R_{pinhole}$, and $R_{ct1}^{pinhole}$ for charge exchange between the gold and electrolyte phases at pinhole sites denote the respective resistances to the ionization of the electron-carrying functional end group, electron transport through the trapped gaseous medium in the pinhole structure, and charge transfer to the underlying gold surface across the work function barrier. An alternative electron flow path for $R_{ct2}^{pinhole}$ is shown by the dotted connection. In this case, $R_{ct2}^{pinhole}$ measures the energy barrier limiting the generation of a free electron by the ionization of electrolyte constituents. (c) Rough gold substrates result in loosely packed monolayer films that facilitate penetration of charge carriers and penetration by charge-exchanging electrolyte constituents. The monolayer−electrolyte interface breaks down in the presence of these large pinholes. (d) The pinhole electrolyte interface lacks a resistance to charge transfer, and the circuit components $R_{pinhole}$ and $R_{ct1}^{pinhole}$ now represent the resistance to charge carriers in the pinhole and the charge transfer resistance across the gold−electrolyte interface in these pinhole sites.

difficulties associated with modeling the complex charge transfer phenomenon in terms of linear circuit elements, such as resistors and capacitors.

The gold−thiol monolayer−electrolyte system depicted in Figure 2 comprises two interfaces: (a) the gold−monolayer interface and (b) the interface between the end of the monolayer chain and the electrolyte solution. Ideally, the $\omega$-functionalized alkanethiols form a symmetric, well-ordered array on the gold surface.[25] The thiol packing density for a close packed monolayer structure with a $\sqrt{3} \times \sqrt{3}$R 30° unit cell on an atomically smooth (111) gold surface results in pinhole sizes that are a fraction (~0.26) of the radius of a gold atom.[40] Surface roughness, inhomogeneties in the substrate, or thermodynamic phase transitions in the thiol molecules during the assembly process can increase the area of the native gold surface that would not be covered by a thiol overlayer.[41] The ions and polar solvent molecules in the electrolyte have to traverse a pinhole bordered largely by hydrophobic surfaces to access the exposed gold surface. In the limiting case when the size of the pinhole is not significantly larger than the diameter of a gold atom, the probability that an ion or water molecule is able to reach the exposed gold area would be very low. As a result, the interface between the functional end group and the electrolyte remains undisturbed. However, the pinhole is conceivably large enough to facilitate penetration by a free electronic charge that can be generated by the ionization of charged or neutral species on the monolayer functional group or in the electrolyte. Another possible path for the transport of charge involves electron transport along the alkane structure of the monolayer phase. Charge transport in the insulating alkane medium can proceed through one of several different mechanisms, such as thermal or field excitation of the charge into the LUMO of the alkane chains,[42] through bond tunneling of the electron along the alkane chain,[19,43] or through thermal hopping of the electronic charge between potential wells localized on carbon atoms of the alkane chain.[44] Thus, a gold−thiol interface characterized by such small pinhole defects can exchange electrons either through the native gold atoms at the pinhole sites or via the gold atoms bound to the thiol moiety of the monolayer (Figure 2a). The transfer of electrons at the site of an exposed gold atom is inhibited by a large potential energy barrier at the surface of the gold atom that arises due to the difference in the chemical

potential of the electrons at the surface of each of the neighboring phases in contact. In the limiting case when solvent molecules are unable to contact the exposed gold area, this energy barrier is approximated by the theoretical work function of gold (~5.4 eV vs vacuum).[42]

However, at the site of a gold−thiol (Au−S) linkage, electrons at the interface are delocalized in the bond orbital that characterizes the linkage, and the chemical potentials of all the bonded electrons at the interface region are equal. Thus, the HOMO level of the monolayer phase is pinned to the gold Fermi level at the gold−monolayer interface. In addition, the Fermi energy of electrons at the gold−monolayer interface, measured with respect to the vacuum energy level shown in Figure 2a, is lower with respect to the same reference than the Fermi energy of surface electrons at a clean gold−vacuum interface because the available states in the surface atoms are now populated by electrons shared by the sulfur moiety.[45,46] Therefore, at the gold−monolayer interface, the gap between the Fermi level of the interface electrons and the bulk monolayer LUMO, denoted by $\Delta$ in Figure 2a, is less than the band gap of the bulk monolayer phase (Figure 2a). At ambient temperatures, higher thermal energies for the electrons in the metal Fermi level further reduce $\Delta$. In addition, electrostatic fields due to (i) dipole and (ii) image charge contributions from the monolayer functional group,[46,47] (iii) the ionic Stern layer, and (iv) the polarization[42,48] induced by the electron density of the alkane medium act to decrease $\Delta$, as described elsewhere in detail.[33] The potential energy barrier to charge transfer for the Au−S site is the sum of the gap between the interface electron Fermi level and the bulk monolayer LUMO ($\Delta$) plus the energy difference between the position of the LUMO at the gold−monolayer interface and the bulk monolayer LUMO ($\Delta E_{LUMO}$). Since the contribution to the potential energy barrier from the $\Delta$ term is negligible compared to the contribution due to the energy difference $\Delta E_{LUMO}$ for the reasons listed above, the electrons transferring across the gold−monolayer interface experience a sharply peaked energy barrier located at the Au−S site, through which they easily tunnel from the gold Fermi level to the bulk monolayer LUMO level or vice versa. Therefore, the gold−monolayer interface behaves as an Ohmic contact,[49] with little or no charge transfer resistance at the Au−S site. We have ignored any difference between the bulk gold and gold−monolayer interface Fermi levels that can also contribute to the electron transfer energy barrier. The assumptions underlying this hypothesis are better justified when the mechanisms for charge transport in the monolayer are described.[33]

The gold−monolayer−electrolyte system, where the monolayer film is ideal and defect free, is represented by an equivalent circuit in Figure 2b. The large potential energy barrier inhibiting the transfer of charge at the gold−pinhole interface can be represented by a charge transfer resistance $R_{ct1}^{pinhole}$. The corresponding charge transfer resistance for electron exchange at the gold−monolayer interface is assumed to be near zero, since the gold−monolayer interface behaves as an Ohmic contact, as discussed above. In addition to the charge transfer barriers at the gold−monolayer and gold−pinhole interfaces, electron transfer from the monolayer−electrolyte interface to the gold−monolayer interface or vice versa is also limited by transport barriers existing within pinhole defects in the monolayer film ($R_{pinhole}$) and within the monolayer phase ($R_{monolayer}$). Thus, the total resistance to an electron in the monolayer phase is either $R_{ct1}^{pinhole} + R_{pinhole}$ if transported through a pinhole defect or $R_{monolayer}$ if the electron gets transported via the alkane chain. The pinhole and hydrocarbon structure in the monolayer also have capacitive contributions ($C_{pinhole}$, $C_{monolayer}$) to their respective total impedance values, which are indicative of their respective charge storage capabilities (Figure 2b). Finally, there is also a barrier to the exchange of electrons at the monolayer−electrolyte interface. In the case of the alkane backbone, the energy barrier limits the electron exchange between the functional end group and specific ions/neutral molecules in the electrolyte ($R_{ct2}^{monolayer}$) that are identified elsewhere.[33] For the pinhole, the potential barrier at the monolayer−electrolyte interface is representative of the amount of energy required for the functional end group to ionize ($R_{ct2}^{pinhole}$) and generate a free electron that can then traverse the pinhole defect (Figure 2b). Alternatively, $R_{ct2}^{pinhole}$ can also represent the energy required to generate a free electron by the ionization of a charged or neutral species in the Stern layer of the electrolyte that can act as the electron donor/acceptor. There is a capacitive contribution ($C_{Stern}$) to the observed impedance due to the monolayer−electrolyte interface since the Stern layer can also store charge.

The equivalent circuit is modified substantially in the limit where pinholes in the monolayer film become large enough to allow electron donating/accepting ions and neutral electrolyte species to have access to the exposed gold sites (Figure 2c). As the pinhole size increases, the hydrophobic "wall" effect associated with the alkane chains that line the pinhole decreases, and as a result, the monolayer−electrolyte interface at the location of the pinhole presents a much smaller barrier to the electrolyte constituents that can exchange charge with the gold sites. Therefore, the resistance to charge transfer at the pinhole−electrolyte interface approaches zero compared to the other impedances; that is, $R_{ct2}^{pinhole} \sim 0$. The total real impedance to charge flow through the large pinhole structure is the sum of (i) the charge transfer resistance at the gold-pinhole interface ($R_{ct1}^{pinhole}$), which now represents the energy barrier to charge transfer between the exposed gold sites and the ionic/neutral charge exchanging electrolyte constituents, plus (ii) the resistance to the transport of these electrolyte species through the pinhole ($R_{pinhole}$) (Figure 2d). The hydrocarbon structure of the monolayer phase is described by the charge transport resistance $R_{monolayer}$, and the monolayer−electrolyte interface adjacent to the alkane structure retains its respective resistive ($R_{ct2}^{monolayer}$) and capacitive ($C_{Stern}$) impedance components as before.

The mechanism of charge transport within an ideal, defect-free monolayer film is most likely going to involve electron transport along the alkane structure. The alternative path for charge flow in a defect-free monolayer film requires the generation of a free electron by the ionization of charged/neutral electrolyte species at the inner or outer Helmholtz planes, transport of the free electron through a pinhole defect, and transfer of the electron across an energy barrier on the order of 5.4 eV at the gold-pinhole interface. This alternative current path is more energy-intensive than the transport of electrons along the alkane chain since the ionization process alone requires energy on the order of 5−10 eV.[50] Thus, the charge transport mechanism in a monolayer film involves two possible alternatives: (1) transport of electronic charge along the alkane backbone of the monolayer phase and (2) penetration of charge donating/accepting electrolyte species within pinhole defects in the monolayer film. The possibility of substantial charged/neutral electrolyte species' penetration within the monolayer phase is significantly diminished if a suitably "smooth" gold substrate is chosen. The hypothesis that electron transport across the alkane phase dominates charge flow through the gold−monolayer−electrolyte system is further supported by the observation that the functional end groups have a significant influence on

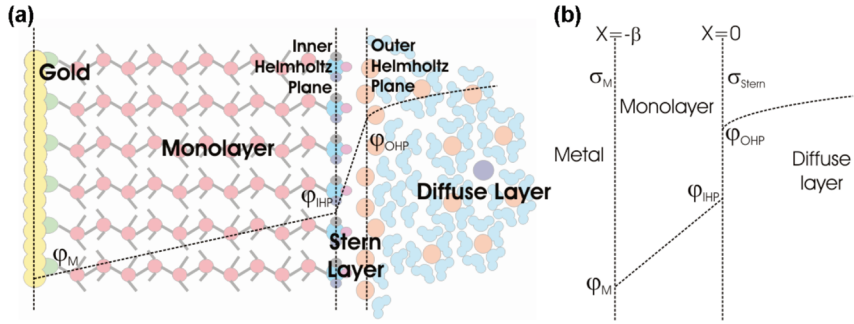


**Figure 3.** (a) Schematic of the double-layer structure at the surface of a monolayer-modified gold electrode in contact with an aqueous electrolyte solution. (b) Electrostatic model of the double-layer structure shown in (a), as used in this work. The inner and outer Helmholtz planes are collapsed to form a single Stern plane with a surface charge density $\sigma_{Stern}$. The potential difference across the Stern plane is given by $\varphi_{IHP} - \varphi_{OHP}$.

the measured transport barrier. In the limit of large pinholes, the effect of the bounding alkane chains and their terminating groups on the transport of electron donating/accepting electrolyte species should be weak, which is opposite the results presented here.

The representation of experimental gold−monolayer−electrolyte systems as equivalent circuits, where the various limiting energy barriers are modeled as linear resistances, presupposes that the barrier height is independent of the monolayer electric field or the applied potential. Since the various energy barriers in both ideal and nonideal gold−monolayer−electrolyte systems contain an electrostatic potential energy contribution due to operating Coulombic forces, the assumption that the charge transport and transfer barriers are independent of applied field is questionable. The resistors in Figures 2b and d can be replaced by nonlinear circuit elements such as diodes or switches that might better represent the nonlinear potential dependent behavior of the limiting barriers in a gold−monolayer−electrolyte system. However, these elements again assume a priori the functional relationship between the barrier height and the applied potential, whereas the actual mechanism by which electronic or ionic charge is transported through the monolayer film is unknown. Thus, a method for the analysis of charge transport in gold−monolayer−electrolyte systems from impedance data must develop a mechanistic description of the process, rather than appeal to a predetermined mechanism by representing the various energy barriers by circuit elements.

Another issue with the equivalent circuits in Figure 2b and d is that they consist of a large number of circuit elements. Thus, the best fit for the observed impedance spectrum of the gold−monolayer−electrolyte system that is obtained by using the frequency response of these equivalent circuits would involve a large number of parameters. The impedance response of the gold−monolayer−electrolyte system shown in Figure 1 can be fit to a reasonable degree of accuracy by a third-order polynomial with respect to frequency. Thus, a minimum of three parameters is required to fit the impedance spectrum of the system adequately. Since the circuit models in Figure 2 b and d involve eight and seven parameters, respectively, the numerical fit for the entire parameter set is likely to be nonunique. An implicit danger in most iterative optimization algorithms used for this purpose is that the final solution obtained is a strong function of the initial choice of values. Therefore, an alternative approach to fit observed impedance values of the gold−monolayer−electrolyte system to a mechanistic description of the charge transfer process is justified, as that will greatly reduce ambiguity in the interpretation of the current and potential observables in an EIS experiment.

**Derivation of the Constitutive Expression for System Admittance.** The gold−monolayer−electrolyte system under consideration (Figure 3a) is modeled as two interfaces at $x = 0$ and $x = -\beta$, bounding a hydrocarbon monolayer phase in between (Figure 3b). This monolayer phase has an absolute dielectric permittivity $\varepsilon$ ($\sim$2.25 $\varepsilon_0$, where $\varepsilon_0 = 8.854 \times 10^{-12}$ $Nm^2/C^2$) [2] and a free charge density, $\rho$. This free charge can be transported through this phase due to an electric potential or chemical potential gradient. The parameters defining electric-field-driven or concentration-gradient-driven transport are the mobility, $\mu$, and diffusivity, $D$, respectively. The interfaces $x = 0$ and $x = -\beta$ that bound the hydrocarbon phase are defined as planes with associated surface charge densities as in the model in Figure 3b, although each interface plane has a finite thickness. The surface charge density at the metal monolayer interface, $\sigma_M$, exists within a finite skin depth ($\delta \sim 0.144$ nm) from the surface of the gold electrode.[51] Similarly, the total charge at the Stern layer is smeared out over the region between the inner and outer Helmholtz planes that are separated by a distance comparable to an ionic radius of the relevant cation or anion (Figure 3a).[52] Since the skin depth at the gold surface and the width of the Stern layer are about an order of magnitude smaller than the length of the hydrocarbon backbone, we can approximate the gold−monolayer and monolayer−electrolyte interfaces as well-defined surfaces, rather than layers of a certain thickness. The diffuse part of the double layer extends beyond the outer Helmholtz plane. In the limit when the current density in the system is small, the equilibrium distribution of ions in this diffuse layer can be described by the classic Poisson−Boltzmann (PB) theory.[52]

Here, we treat the gold−monolayer−electrolyte system as a leaking parallel plate capacitor, in which the two plates of the capacitor are defined by the gold−monolayer and the monolayer−electrolyte interfaces (Figure 3b). A potential is applied to the monolayer-modified gold surface (working electrode) with respect to a reference in the bulk electrolyte solution, where this bias drops across the leaky capacitor and the neighboring diffuse layer, resulting in a net flow of charge between the reference and working electrode. At steady state, the current density in the monolayer region is equal to net current density in the system. The constitutive equation describing the current density in the monolayer phase can be given as[10]

$$J = \sigma E - D\frac{\partial \rho}{\partial x} + \varepsilon \frac{\partial E}{\partial t} \qquad (1)$$

where $\sigma$ is the conductivity of the alkane region, $E$ is the resultant local electric field in the monolayer, and $\rho$ is the free charge density in the hydrocarbon phase. The quantities $\mu$, $D$, and $\varepsilon$ are the mobility and diffusivity of the charge carriers and

the dielectric permittivity in the monolayer phase, respectively. The conductivity can be rewritten as $\sigma = \mu\rho$, thus redefining the conductive current as $\rho v_{drift}$, where the drift velocity of the charge carriers is defined as $v_{drift} = \mu E$.[42] Later, this linear dependence of $v_{drift}$ on $E$, referred to as the Helmholtz−Smoluchowski approximation, will be justified. Note that eq 1 is not restricted to any specific mechanism of charge transport within the monolayer phase; it is equally applicable to the case when charge is transported via ion migration through pinhole defects or when charge flow is due to electron flow through the alkane phase of the monolayer film. Since the charge transfer process between the gold Fermi level and the electron donating/accepting electrolyte species is nonadiabatic due to the intervening monolayer film, the description of the observed current density as a charge flux though the monolayer film in eq 1 is expected to hold over a substantial part of the potential range of interest. This assumption breaks down when wavelike properties of the transported electronic charge begin to manifest themselves or where the observed current density is limited by the rate at which the dielectric acquires a favorable nonequilibrium conformation to facilitate charge transfer; that is, when the charge transfer reaction becomes adiabatic. The potential regimes where these exceptions occur are described elsewhere in detail.[33] Thus, for most of the potential range of interest, neither a description of the reaction kinetics of the actual electron transfer at the monolayer−electrolyte interface nor the precise identity of the species participating in the interface reaction are required when we use eq 1 to describe charge transfer in these electrochemical systems. Equation 1 when transformed into frequency space yields

$$J(\omega) = \mu\rho(\omega)\, E(\omega) - D\,\frac{\partial\rho(\omega)}{\partial x} + i\omega\varepsilon E(\omega) \qquad (2)$$

The properties of the monolayer region, namely $\mu$, $D$, and $\varepsilon$, are assumed to be frequency-independent in eq 2. The assumption that the properties of the monolayer phase are independent of frequency and the assumption of the existence of quasi-steady-state conditions limits the use of eq 2 to low frequencies ($\omega < D/\beta^2$). Differentiating eq 2 with respect to the applied potential bias ($\varphi_M$) gives a constitutive expression for the total admittance of the system, resulting in

$$Y_{sys}(\omega) = Y_{sys}^{Re} + iY_{sys}^{Im} = \frac{\partial J(\omega)}{\partial\phi_M} = \frac{\partial}{\partial\phi_M}\left(\mu\rho E - D\,\frac{\partial\rho}{\partial x}\right) + i\omega\,\frac{\partial}{\partial\phi_M}(\varepsilon E) \qquad (3)$$

Because none of the physical properties of the system are frequency dependent, we can separate out the real and imaginary parts in eq 3, such that

$$Y_{sys}^{Re} = \frac{\partial}{\partial\phi_M}\left(\mu\rho E - D\,\frac{\partial\rho}{\partial x}\right) \qquad (4a)$$

and

$$\frac{Y_{sys}^{Im}}{\omega} = \frac{\partial}{\partial\phi_M}(\varepsilon E) \qquad (4b)$$

The admittance of the system can be derived from the observed impedance data as the reciprocal of the impedance after discounting for the IR drop in the bulk electrolyte solution. The solution resistance ($R_s$) needed to calculate the IR drop is obtained from the high frequency intercept of the Nyquist plot at the real axis.[10] Therefore, the real and imaginary parts of the system admittance are given by

$$Y_{sys}^{Re} = \frac{(Z_{sys}^{Re} - R_s)}{(Z_{sys}^{Re} - R_s)^2 + (Z_{sys}^{Im})^2} \qquad (5a)$$

and

$$Y_{sys}^{Im} = \frac{-Z_{sys}^{Im}}{(Z_{sys}^{Re} - R_s)^2 + (Z_{sys}^{Im})^2} \qquad (5b)$$

Integrating eqs 4a and 4b with respect to the applied potential $\varphi_M$ yields

$$\int_0^V Y_{sys}^{Re}\,\partial\phi_M + I_{V=0} = \mu\rho E - D\,\frac{\partial\rho}{\partial x} \qquad (6a)$$

and

$$\int_0^V \frac{Y_{sys}^{Im}}{\omega}\partial\phi_M + Q_{PZF\to 0} = \varepsilon E \qquad (6b)$$

The integration constants $I_{V=0}$ and $Q_{PZF\to 0}$ are the measured DC current and the amount of charge stored on the gold surface at zero applied bias. The transport parameters ($\mu$, $D$) and dielectric permittivity ($\varepsilon$) are assumed to be independent of the resultant electric field in the monolayer phase, thereby making the problem analytically tractable. For a specific value of applied DC potential ($\varphi_M = V$), the local electric field in the monolayer ($E$) can be obtained from eq 6b, and this value of $E$ is an input into the first order differential equation in 6a, which can be used to calculate $\rho$. Equation 6b implies that the product $\varepsilon E$ is independent of position. If the dielectric permittivity for the monolayer phase is a constant, this would suggest that the local electric field, $E$, is invariate with position in the monolayer phase. This observation will be analyzed in greater detail in the next section. The parameters $E$ and $\rho$ are dependent on the integrated path in potential space, and this path is uniquely determined by the admittance of that particular gold−monolayer−electrolyte system.

An important outcome of this analysis is the determination of the PZF, which denotes a specific value of potential at which the resultant electric field in the system goes to zero. We hypothesize that this point is unique to the particular gold−monolayer−electrolyte system under investigation and that, like the concept of the potential of zero charge,[52] only one such point can exist in the potential spectrum.[53] Since the electric field in the monolayer phase reduces to zero at the PZF, the gradient of electrostatic potential extends over a very large length scale in the gold−monolayer−electrolyte system (i.e., $\partial\varphi_M/\partial E \to \infty$). Thus, the PZF corresponds to the potential at which $\partial E/\partial\varphi_M = 0$, and the electric field at this point is set to zero at that potential. All gold−monolayer−electrolyte systems that were investigated did not exhibit any local maxima/minima. The monotonic variation of the electric field with potential away from the PZF supports our hypothesis that the PZF is a unique characteristic of a particular electrochemical system. Note, however, that even though the conductive current is zero at the PZF, a diffusive contribution to the total current still exists.

The first-order differential equation in eq 6a can be integrated and solved for $\rho$, once $E$ is calculated from eq 6b. The solution is contingent upon knowing the appropriate boundary condition either at $x = 0$ or $x = -\beta$. A significant potential energy barrier to charge transfer, either at $x = 0$ or $x = -\beta$, gives rise to a large intrinsic electric field at these locations, which results in a discontinuity in the charge density at each interface. Therefore, the value of $\rho$ at $x = -\beta + \zeta$ or at $x = 0 - \zeta$ ($\zeta > 0$; $\zeta \to 0$) would then be unknown. However, in the limiting case, when the gold−monolayer interface behaves as an Ohmic contact

without a significant potential energy barrier and the electric field in the monolayer film is independent of the location within the monolayer film, the boundary condition becomes

$$\rho(x = -\beta) = \frac{\sigma_M}{\delta} \tag{7}$$

where the term $\delta$ is the skin depth of the gold surface ($\sim$0.144nm)[51] over which the metal surface charge density, $\sigma_M$, occurs, which can be estimated from the electric field, as shown in the next section. Note that the assumption of the gold−monolayer interface barrier being negligible appears only in the evaluation of $\rho$. Therefore, the boundary condition (eq 7) is applicable for the case when the underlying gold substrate is sufficiently smooth such that the pinhole contribution to the observed current density can be ignored, as we will demonstrate in the Results and Discussionsection. The calculation of the electric field in the monolayer, on the other hand, relies only on the assumption that quasi-steady-state conditions prevail with respect to the excitation frequency, $\omega$.

**Effect of Finite Charge Size on the Calculated Electric Field and Estimation of $\sigma_M$.** Gauss' law relates the net electric field ($E$) to the volume free charge density ($\rho$) in the monolayer phase, such that

$$\frac{\partial(\varepsilon E)}{\partial x} = \rho + \rho_b \tag{8}$$

Integrating this expression from $x = -\beta$ to some general point $x$ within the monolayer phase yields

$$\varepsilon E = \int_{-\beta}^{x} (\rho + \rho_b)\, dx + \sigma_M \tag{9}$$

Equation 9 gives a pseudo monolayer surface charge density ($\varepsilon E$) that varies with position in the monolayer film. However, a spatially varying monolayer surface charge density is clearly at odds with eq 6b and violates the principle of charge conservation under the quasi-steady-state assumption. Here, we maintain charge conservation by treating the charges in the monolayer phase as discrete entities where each charge excludes the others from its immediate neighborhood by Coulomb repulsion. The discrete nature of charge carriers is modeled using a cutoff sphere approach as previously used by Levine et al., in which each charge is surrounded by an exclusion sphere of radius $R$ such that the charge density is nonzero only outside this sphere.[54,55] Barlow et al. provided an estimate for the value of $R$ by assuming that charges mimicked the packing arrangement of the underlying substrate and organized themselves into a latticelike structure in the lateral ($y-z$) plane.[56] As per their calculations,

$$R = 4.301 \times 10^{-7} (1/\sigma_a)^{1/2} \tag{10}$$

where $R$ is in centimeters and $\sigma_a$ is the charge density in the lateral plane in microcoulombs per square centimeter. In the limit that we have a perfect monolayer structure in which every alkane chain hosts a unit free or bound charge, the radius of the exclusion sphere, $R$, is 3 Å. Thus, a charge in the monolayer phase has very few neighbors in the $x$ direction when the thickness of the film is only a couple of nanometers. The electric field "seen" by this charge is determined primarily by the surface charge density at the gold−monolayer interface. Thus, by setting $\rho \sim 0$, eq 9 can be rewritten as

$$\varepsilon E = \sigma_M \tag{11}$$

Expression 11 assumes that the gold phase lacks a significant intrinsic electric field as a result of an intrinsic potential energy barrier to charge transfer that arises due to a difference between the bulk and surface gold Fermi levels. The validity of the assumption underlying 11 (namely that the charges are discrete entities) can be tested by checking to see if eq 11 violates the principle of charge conservation. Charge conservation in 1-D requires that

$$\frac{\partial J}{\partial x} = \frac{\partial}{\partial x}\left(\mu\rho E - D\frac{\partial \rho}{\partial x}\right) + i\omega \frac{\partial}{\partial x}(\varepsilon E) = 0 \tag{12}$$

At steady state, the DC component of the total current would be invariant with $x$, and therefore,

$$\frac{\partial}{\partial x}(\varepsilon E) = 0 \tag{13}$$

Thus, eq 11 obeys overall charge continuity and is a convenient tool for the evaluation of $\sigma_M$.

**Estimation of Charge Mobility and Diffusivity.** The solutions to eqs 6a and 6b are possible only if the transport properties of charge carriers in the monolayer phase ($\mu$, $D$) are known. A few papers have reported on the low-field conductivity values of alkanethiol monolayers sandwiched between two metal junctions.[57,58] However, to our knowledge, the variation of alkane chain conductivity over a wider range of applied electric fields has not been described. The topic of thermal diffusion of charge carriers through the monolayer phase of a gold−monolayer−electrolyte system also has not been dealt with quantitatively. Here, we estimate the charge mobility and diffusivity in the monolayer phase at the order-of-magnitude level using a scaling analysis. The constitutive charge transport eq 1 is split into its real and imaginary components and nondimensionalized to yield

$$\left(\frac{J_o X}{D\rho_o}\right)\underline{J}^{DC} = \left(\frac{\mu E_o X}{D}\right)\underline{\rho}\,\underline{E} - \frac{\partial \underline{\rho}}{\partial \underline{x}} \tag{14a}$$

and

$$\left(\frac{Q_o}{\varepsilon E_o}\right)\underline{Q}^{AC} = \underline{E} \tag{14b}$$

The quantities $\underline{J}^{DC}$, $\underline{Q}^{AC}$, $\underline{E}$, $\underline{\rho}$, and $\underline{x}$ are the nondimensional DC current, gold surface charge density, electric field, monolayer free charge density, and length, respectively; $J_o$, $Q_o$, $E_o$, $\rho_o$, and $X$ are their characteristic scaling parameters, respectively. The quantities $\mu$, $D$, and $\varepsilon$ are the mobility and diffusivity of the charge carriers and the dielectric permittivity in the monolayer phase, respectively. The scaling parameters are chosen such that the nondimensional values vary between 0 and 1. Thus,

$$J_o = \max\left(\int_0^V Y_{sys}^{Re}\, \partial\phi_\beta + I_{V=0}\right) \tag{15a}$$

and

$$Q_o = \max\left(\int_0^V \frac{Y_{sys}^{Im}}{\omega}\, \partial\phi_\beta + Q_{PZC\to 0}\right) \tag{15b}$$

The value of $E_o$ can then be evaluated from eq 14b because the quantity between brackets on the left-hand side must be of order 1 for the equality to hold. The nondimensional number $\mu E_o X/D$ in eq 14a is a measure of the relative strength of the conduction to the diffusion current. At large electric fields ($\sim E_o$) and at room temperatures ($kT \sim 25$ meV), the two mechanisms of charge transfer are expected to contribute equally to the total current. For weaker electric fields ($\ll E_o$), diffusion currents are expected to dominate, and the nondimensional ratio will be much less than 1. The characteristic scale for the volume charge

density in the monolayer can be obtained by nondimensionalizing Gauss' law, giving

$$\underline{\rho} = \left(\frac{\varepsilon E_o}{X\rho_o}\right)\frac{\partial \underline{E}}{\partial \underline{x}} \tag{16}$$

As in eq 14b, $\rho_o$ must be equal to $\varepsilon E_o/X$ for the equality to hold. Substituting this expression for $\rho_o$ into eq 14a provides order-of-magnitude estimates for the diffusivity, $D$, and charge mobility, $\mu$, in the monolayer phase

$$D \sim \frac{J_o X^2}{\varepsilon E_o} \tag{17a}$$

and

$$\mu \sim \frac{J_o X}{\varepsilon E_o^2} \tag{17b}$$

The values of $J_o$ and $E_o$ can be evaluated from eqs 15a and 15b, respectively, and the length scaling parameter, $X$, is considered comparable to the monolayer film thickness, $\beta$. The choice of the monolayer film thickness, $\beta$, as the length scaling parameter is justified elsewhere, where the different mechanisms of charge conduction are discussed in detail.[33] The diffusivity and mobility calculated using this method are $10^{-17}$ ($m^2/s$) and $10^{-18}$ ($S\cdot m^2/C$), respectively. We will demonstrate agreement between the value of mobility derived here and those values measured at low-field conductivity described elsewhere.[57,58] The scaling methodology described here also demonstrates the applicability of the constitutive form of the conduction current chosen here. An expression for the conductive current of the form $J_{cond} = \sigma E = \mu\rho E^n$, where $n > 1$, results in a value of the charge mobility that is significantly smaller than $10^{-17}$ ($m^2/s$). The conductivity calculated from this value of mobility will be in poor agreement with the reported low-field conductivity of the alkane films. In summary, recording low-frequency admittance as a function of the DC bias at the working electrode enables the calculation of parameters ($\rho$, $E$) from eqs 6a and 6b that characterize charge transport within the monolayer.

## Experimental Details

**Preparation of Monolayer Surfaces.** *n*-Alkyl thiols ($CH_3(CH_2)_n-SH$, $n$ = 9, 10, 11, 14, 15, 17), 11-mercaptoundecanoic acid, 16-mercaptohexanoic acid, and 11-mercapto-1-undecanol, all purchased from Sigma Aldrich, were dissolved in absolute ethanol (Pharmaco-Aaper, Shelbyville, KY) at a concentration of 1 mM. Long alkane chain thiol molecules, such as 1-octadecane thiol (Sigma Aldrich, St. Louis, MO), that were only partially soluble in ethanol were dissolved in a 2:3 mixture of toluene (analytical grade, Sigma Aldrich, St. Louis, MO) and absolute ethanol. SPR quality glass slides (GenTel Biosciences, Madison, WI) coated with evaporated chrome (5 nm) and gold (100 nm) thin films were washed in a heated SC-1 bath (100 mL of DI water/25 mL of $H_2O_2$/2 mL of $NH_4OH$) and rinsed thoroughly with DI water (resistivity 18 MΩ-cm) and ethanol. The high resistivity of the DI water used here, which is comparable to the resistivity of Millipore water, indicates that the water is relatively free of metallic and ionic contaminants. These gold surfaces were left to incubate in a Parafilm-sealed beaker in the respective solutions of thiol molecules for 48 h in a class 1000 cleanroom. The resulting thiol-coated surfaces were rinsed thoroughly with ethanol and DI water and blow-dried with dry $N_2$ before use. XPS on the monolayer-modified surfaces was performed with a Kratos Axis ULTRA X-ray photoelectron spectrometer using an Al X-ray source at 225 W, and the spectra were compared with published data[59,60] to verify the presence of the monolayer film.

**Substrate Preparation for Surface Area Studies.** The gold-coated glass slides were cleaned in a hot SC-1 bath as before, thoroughly rinsed in DI water, and blow-dried with dry, inert $N_2$ before use. The glass slides were used as-is for the contact angle measurements and the gold oxide reduction experiments. Care was taken to minimize the exposure of the gold surface to the ambient prior to the actual experiment. For the iodine desorption experiment, the gold surface was pretreated with iodine by exposing the slide to 1 mM sodium iodide (Sigma Aldrich, St. Louis, MO) in 1 M $H_2SO_4$ (99.9%, Sigma Aldrich, St. Louis, MO). The iodine-treated gold surface was rinsed with 1 M $H_2SO_4$ before running the potential cycle for desorption. Thiol desorption studies were conducted using 1-decane thiol (Sigma Aldrich, St. Louis, MO)-coated gold surfaces that were prepared as specified.

**Contact Angle Measurements.** The advancing ($\theta_A$) and receding ($\theta_R$) contact angles were measured using a goniometer (CAM 100, KSV, Finland). A high-speed camera (DMK 21F04, Imaging Source Inc., Charlotte, NC) was used to visualize the experiments at 30 frames/s. The experiments were conducted in a class 10 cleanroom environment at a relative humidity of 34%. Drop shape analysis software (KSV, Finland) was used to calculate the wetting angles. The results for the SC-1 cleaned gold surface are as follows: $\theta_A = 10° \pm 3°$, $\theta_R = 8° \pm 3°$.

**Electrochemical Instrumentation and Measurements.** Electrochemical measurements were performed using a GAMRY Femtostat (Gamry Instruments, Warminster, PA) employing a three-electrode cell: the monolayer-coated gold surface acted as the working electrode, an Ag/AgCl wire in 3 M KCl (Bioanalytical Instruments, West Lafayette, IN) as the reference, and a gold or platinum wire as the counter electrode. Platinum was used as the counter electrode for all surface area measurements and for a few of the impedance experiments. Gold counter electrodes were used for most of the impedance measurements. The effect of the material and diameter of the counter electrode was found to be insignificant when impedance experiments with different counter electrodes were compared. All potentials are reported with respect to the Ag/AgCl reference. The working electrode was clamped in position using a vertical stage such that a constant area of the gold slide was immersed in the electrolyte solution. Electrolyte solutions for the impedance experiments were prepared as a ratio of mono- and dihydrogen potassium phosphate salts (ACS reagent grade 99.99%, Sigma Aldrich, St. Louis, MO) in DI water (resistivity 18 MΩ-cm) such that the total salt concentration and pH of the bulk electrolyte were as desired. All electrolyte solutions were degassed with nitrogen for an hour prior to the experiment. The potential spectrum of the low frequency impedance values was recorded by stepping the DC bias through increments of 25 mV over the range of −500 to 500 mV. The remaining points in the spectra plotted here are obtained by a cubic spline interpolation[61] between the recorded data. We verified the accuracy of the spline interpolation by reducing the increment size to 5 mV in the neighborhood of the PZF obtained from the interpolated curve. The PZF realized from the smaller increments differs from the interpolation result by ±5 mV. This error includes the variance due to composition of the electrolyte, electrode variability, and the error due to the interpolation curve. The DC potential range considered here is within the range of electrochemical stability of the thiols.[62] Electrochemical desorption of the thiols is characterized by a rapid decrease in

impedance for a small change in potential, and destruction of the monolayer film changes the impedance characteristics of the solid−liquid interface. Thus, impedance spectra at lesser anodic/cathodic potentials can no longer be repeated. These observations were used as checks to ensure that the anodic/cathodic desorption thresholds were not crossed.

## Results and Discussion

In this paper, we apply the methodology described in the previous sections to determine two physicochemical characteristics of the interface between the monolayer functional groups and the electrolyte solution: (i) the built-in electric field and (ii) the equilibrium chemical potential difference between the metal and the inner Helmholtz plane for a charge carrier. We demonstrate that these characteristics are specific to the gold−monolayer−electrolyte system under consideration. Therefore, they provide valuable insights into the electronic properties of the monolayer−electrolyte interface. The gold−monolayer−electrolyte system is also shown to be qualitatively analogous to a solid state Mott−Schottky barrier due to the existence of these two characteristics and also because of the anisotropic nature of the current−potential curves around the potential of zero electric field.

**Surface Area Measurements.** The true surface area of the gold substrate underlying the adsorbate is calculated from the total charge exchanged between the gold surface and the electrolyte solution in a well-characterized surface reaction. The surface roughness, $r$, is then estimated by comparing the experimentally determined electrolytic charge with the theoretical amount of charge transferred when the reaction proceeds on an ideal, flat surface, such that

$$r = \frac{A_{\text{true}}}{A_{\text{geometric}}} = \frac{Q_{\text{experimental}}}{Q_{\text{theoretical}}} = \frac{Q_{\text{experimental}}}{A_{\text{geometric}} \cdot \sigma_{\text{theoretical}}} \tag{18}$$

The surface reactions considered here involve the chemisorption or desorption of a particular species (iodine, oxygen, 1-decane thiol) on the gold substrate, and the theoretical calculation of total charge typically involves an assumption about the packing density of the adsorbate on the gold surface.

Iodine atoms are known to chemisorb on gold in a hexagonal, close packed arrangement where the average packing density ($\Gamma_{\text{avg}}$) of the atoms is given by[63]

$$\Gamma_{\text{avg}} = \frac{1}{2\sqrt{3} r_{\text{VDW}}^{2} N_{\text{A}}} \tag{19}$$

where $N_{\text{A}}$ is Avogadro's constant and $r_{\text{VDW}}$ represents the van der Waals radius of the iodine atom in the above expression ($r_{\text{VDW}} \sim 0.215$ nm). The chemisorbed iodine can be anodically oxidized to aqueous $IO_3^-$ by the application of a potential at the gold surface, such that

$$I_{(\text{ads})} + 3H_2O \rightarrow IO_3^- + 6H^+ + 5e^- \tag{20}$$

Thus, the measured surface area of the gold surface is[63]

$$A = \frac{(Q - Q_{\text{ox}})}{5F\Gamma_{\text{avg}}} \tag{21}$$

The charge, $Q$, obtained by integrating the iodine oxidation peak 1 in Figure 4a is corrected for the accompanying gold oxidation charge, $Q_{\text{ox}}$, in peak 2 that is seen in the voltammetric scans for both the iodine-pretreated (Figure 4a) and clean gold surfaces (Figure 4b).

Gold forms various oxides ($Au_2O_3$, $Au(OH)_3$), with different stoichiometric ratios and physical properties, at characteristic anodic potentials in a phosphate buffer at pH 7.[64] Oesch et al. calculated the total charge required to completely oxidize the surface of a polycrystalline gold substrate to $Au_2O_3$ using the fact that the (111) plane has 60% higher surface concentration than the (110) plane.[65] This theoretical charge density of 723 $\mu$C/cm$^2$ is compared to the charge obtained by integrating the oxidation peak (1) in Figure 4c. The oxide film so formed can be reduced at sufficiently cathodic potentials as

$$Au_2O_3 + 3H_2O + 6e^- \rightarrow 2Au + 6OH^- \tag{22}$$

Given the bulk density for $Au_2O_3$ ($\rho_{\text{oxide}} = 11$ gm/cm$^3$), Oesch et al. calculated the thickness of the oxide film ($d_{\text{oxide}}$) as 4.7 nm.[65] Thus, from eq 22, the theoretical charge per unit area required for the reduction of the oxide film can be evaluated as

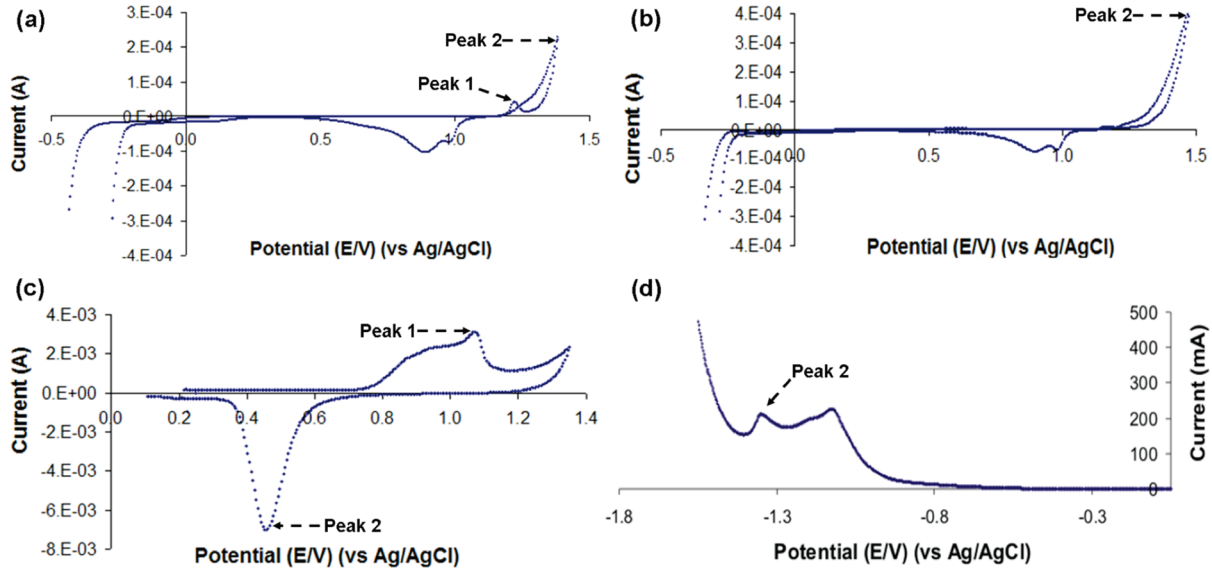


**Figure 4.** Cyclic voltammograms of (a) an iodine-pretreated and (b) a clean, polycrystalline gold substrate in 1 M $H_2SO_4$ solution at a scan rate of 3 mV/s and (c) a clean polycrystalline gold substrate in a 0.5 M phosphate buffer solution maintained at pH 7 for a scan rate of 100 mV/s. (d) Linear sweep voltammogram at 50 mV/s for the reductive desorption of a 1-decanethiol monolayer from polycrystalline gold in 0.5 M KOH.

$$\sigma_{red} = \frac{6\,F\rho_{oxide}d_{oxide}}{M_{oxide}} = 677\,\mu C/cm^2 \quad (23)$$

where $F$ and $M_{oxide}$ are Faraday's constant and the molecular weight of the oxide film, respectively. The ratio of the charge calculated from eq 23 to the charge obtained by integrating the reduction peak (2) in Figure 4c gives the roughness ratio, $r$.

Surface roughness can also be estimated by measuring the total electrolytic charge exchanged between the gold and the monolayer molecules in the reductive desorption of 1-decanethiol from the gold substrate. The desorption of alkanethiol monolayers at cathodic potentials proceeds by the following mechanism in a 0.5 M aqueous KOH electrolyte,[66] where

$$AuSR + e^- \rightarrow Au(0) + RS^- \quad (24)$$

On the basis of the mechanism described in reaction scheme 24, the theoretical amount of charge required for desorbing an ideal monolayer film on a (111) single crystal gold surface is

$$\sigma_{desorption} = \frac{e}{A} \quad (25)$$

Assuming that the thiol molecules pack ideally in a $\sqrt{3} \times \sqrt{3}$R 30° unit cell at the gold surface, the area occupied by one thiol molecule ($A$) is evaluated to be ~21.6 Å$^2$.[3] The theoretical charge so calculated assumes a single crystal gold surface. However, a flat polycrystalline gold surface with (110) facets mixed with (111) crystal planes would exhibit a lower surface area than a substrate that is purely (111).[65] Thus, the theoretical charge density at the polycrystalline surface is expected to be lower. The voltammetric scan in Figure 4d exhibits the characteristic two-peak wave that is associated with desorption of thiol molecules from (111) and (110) facets of the polycrystalline surface.[67] After subtracting the capacitive charging current and baseline correction before peak 2, the charge required for monolayer desorption can be estimated by integrating the voltammetric curve between −0.4 and −1.4 V. The roughness calculated from the ratio of the measured desorption charge to the theoretical charge released at an ideal (111) single crystal gold surface is expected to be less than the actual roughness because the theoretical charge density at a polycrystalline surface is lower, as discussed above.

The roughness ratios of the polycrystalline gold substrate evaluated from these three different electrochemical experiments are listed in Table 1. The data indicates that the difference between the actual and geometric surface areas is small, and the substrate can be considered smooth. The measurements of the advancing ($\theta_A = 10° \pm 3°$) and receding ($\theta_R = 8° \pm 3°$) contact angles on the gold surface also display little hysterisis, indicating that the native gold surface is flat. However, the process of functionalizing the gold surface with the alkane thiol film seems to increase the substrate roughness, as indicated by the increased area ratio measured from the electrochemical desorption of the film. The electrochemical desorption of thiols from the gold substrate also reveals the dual peak voltammetric wave that is indicative of the polycrystalline structure of the underlying surface. However, given that the roughness ratio is close to 1, we assume that pinhole defects do not play a significant role in the transfer of charge between the gold and the electrolyte. This assumption will be reexamined in the discussion of the effect of monolayer thickness and end group on the charge transfer process.

**Calculation of Low-Field Conductivity.** The average conductivity of the monolayer film ($\sigma_{cond}$) in the Helmholtz−Smoluchowski limit is defined as

$$\sigma_{cond} = \frac{\mu}{\beta}\int_{-\beta}^{0}\rho(x)\,dx \quad (26)$$

In the low-field limit, the conductivity is independent of the thickness of the monolayer (Figure 5) and is on the order of $10^{-13}$ S/m. This result compares very well with reported low-field conductivity values of alkanethiol monolayers bridging two metal junctions (~$10^{-15}$ S/cm),[57,58] thus indicating that the scaling approach we use here to evaluate the mobility and diffusivity of charge carriers in the monolayer phase is accurate in at least one asymptotic limit. The close correspondence between the calculated low-field conductivity in this paper and the reported values for the conductivity of an alkane film indicates that charge flow through the system is primarily due to the transport of electrons through the alkane phase and is not affected by the transport of ions through pinholes, particularly since the scaling analysis for the calculation of charge mobility, $\mu$, does not a priori define a specific mechanism of charge transport within the monolayer structure.

**Qualitative Analogy between Mott−Schottky Barrier and Gold−Monolayer−Electrolyte System.** Figure 6a depicts the absolute value of the electric field in the monolayer phase as a function of the applied potential and different bulk electrolyte pH values for a carboxylic acid terminated monolayer that is 10 sp$^3$ hybridized methylene moieties long (~1.4 nm).[58,68] The electric field reduces to zero at a characteristic value of the applied potential and is otherwise monotonic in behavior at potentials that are more anodic or more cathodic than this characteristic potential. This potential is called the potential of zero field ($V_{PZF}$). Although eq 11 indicates that the charge on the metal ($\sigma_M$) would also be zero at this voltage, we refrain from referring to this value of potential as the potential of zero charge ($V_{PZC}$). The assumption of finite charge size underlying eq 11 makes $V_{PZF} = V_{PZC}$, although in reality, a small difference between the two potential values would arise from the error in the finite charge size assumption. Another characteristic of interest in the gold−monolayer−electrolyte system, such as the PZF, is the built-in or residual electric field ($E_{bi}$), which is the nonzero value of the electric field at zero applied potential (Figure 6a). An electric field of significant magnitude (~$10^8$

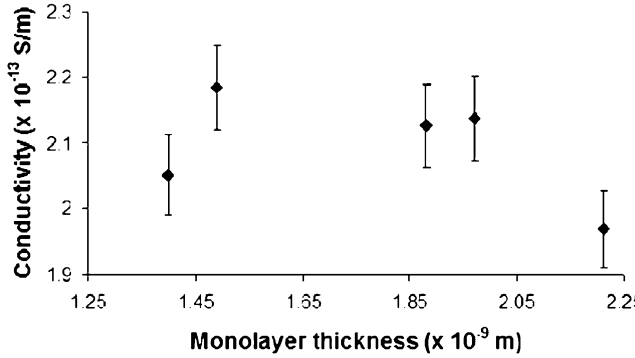


**Figure 5.** Low-field monolayer conductivity for methyl-functionalized monolayer films with a varying number of methylene units in the alkane backbone. The electrolyte is a 10 mM phosphate buffer solution maintained at pH 8.

**TABLE 1: Roughness Ratios As Obtained from Multiple Experimental Techniques**

| experimental technique | roughness ratio ($r$) |
|---|---|
| desorption of chemisorbed iodine | 1.24 |
| oxidation of gold surface to $Au_2O_3$ | 1.15 |
| reduction of gold oxide ($Au_2O_3$) | 1.10 |
| reductive desorption of 1-decanethiol monolayer | 1.46 |

V/m) that exists in a gold−monolayer−electrolyte system with no applied bias characterizes the distortion of the HOMO and LUMO band profiles at the monolayer−electrolyte interface in the absence of an externally imposed field, such that

$$\phi_M - \phi_{IHP} = -\phi_{IHP} = E_{bi}\beta \quad (27)$$

We make use of the finite charge size assumption in eq 13 to postulate a linear potential drop for the monolayer phase in eq 27. Thus, the residual electric field (or the IHP potential at zero applied bias) in the system is an electrostatic property intrinsic to a specific monolayer−electrolyte interface. The net current density−voltage characteristics of the systems in Figure 6a are depicted in Figure 6b and as a semilog plot in Figure 6c. The trends in the current density are anisotropic about $V_{PZF}$, and the rapid increase in current density for $V < V_{PZF}$ is clearly visible. These three properties (namely, (a) a built-in electric field in the monolayer, (b) the fact that the electric field in the monolayer can be tuned to zero with applied potential, and (c) the large increase in current density with applied bias for potentials that are more cathodic than the PZF) are common to a gold−monolayer−electrolyte system and a solid state Schottky barrier.[42,69,70] As discussed before, both a charge transport barrier within the monolayer phase and a barrier to the transfer of charge across the monolayer−electrolyte interface limit the flow of charge in a gold−monolayer−electrolyte system. These potential energy barriers arise due to the differences in chemical potentials of the electrons in the metal and at the inner Helmholtz layer and between the electron at the inner Helmholtz plane and the electrolyte phase, respectively (Figure 2). Similarly, the current flow in a Schottky junction between a metal and

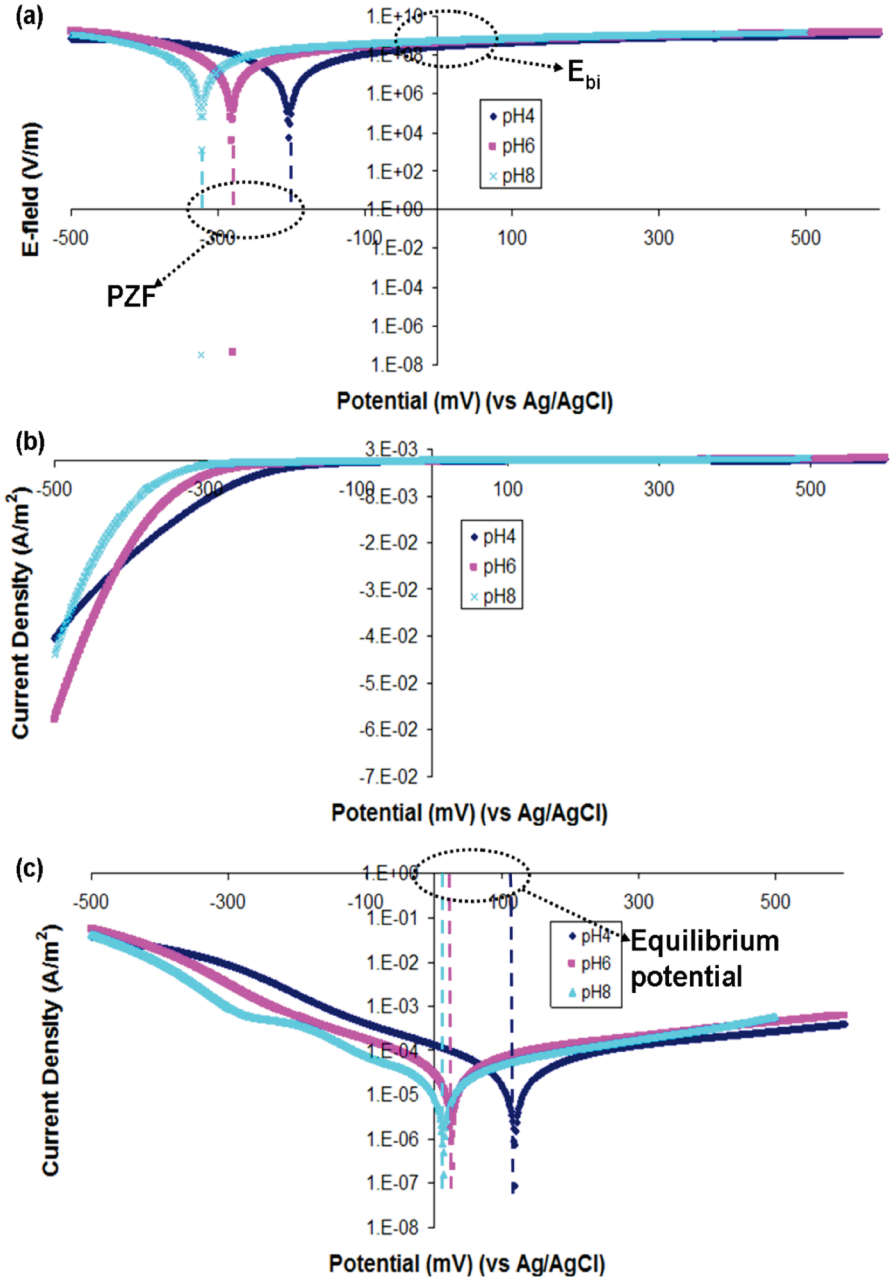


**Figure 6.** (a) Monolayer electric field and (b, c) net current density are plotted as functions of applied potential. The net current density is depicted as the semilog plot in c to demonstrate the existence of the nonequilibrium potential, which is not immediately evident in graph b. Note that the zero applied bias and equilibrium conditions occur at potentials that are more anodic than the PZF. For all systems, a self-assembled monolayer film of 1-mercaptodecanoic acid on gold is the working electrode unless otherwise mentioned. The electrolyte phase consists of 10 mM phosphate buffer solutions maintained at different pH values of 4, 6, and 8.

semiconductor phase is limited either by the rate of charge transport in the semiconductor phase or the rate of electron transfer at the metal−semiconductor interface. The potential energy barriers limiting charge flow in a Schottky junction and the free energy barriers limiting current flow in a gold−monolayer−electrolyte electrochemical system can be tuned by the application of a potential bias, which gives rise to a characteristic potential where the net electric field reduces to zero.[42,69,70] The built-in field in a Schottky junction is also a measure of the intrinsic potential energy barrier that inhibits the transfer of charge across a heterogeneous metal−semiconductor interface, similar to the built-in field for a gold−monolayer−electrolyte system.[42,69,70] However, the similarities between a Schottky junction and a gold−monolayer−electrolyte system are qualitative only, since the mechanism of charge transport across a nanometer-thick monolayer phase is significantly different from charge transport in a semiconductor, such as silicon. In addition, the charge transfer across a semiconductor−metal interface involves a direct interaction between the electronic orbitals of a metal and semiconductor, where both materials can carry appreciable numbers of free electrons at room temperatures ($\sim 10^3$ cm$^{-3}$ for silicon). However, in the case of a monolayer−electrolyte interface, the process of charge transfer is usually accompanied by vibrational excitation of occupied states of ionic/neutral electrolyte species that can act as electron donors or acceptors, since there are a negligible number of free electrons in an electrolyte solution.

The free energy of the electron in a specific phase is related to its electrochemical potential as[45]

$$\frac{\partial G^i_{\text{total}}}{\partial n} = \underline{\mu}^i_e = \mu^i_e - e\phi^i(x) \tag{28}$$

where the terms $G^i_{\text{total}}$, $\underline{\mu}^i_e$, and $\mu^i_e$ are the free energy, electrochemical potential, and chemical potential of the electron respectively, and $\varphi^i(x)$ is the inner potential of the phase $i$ in which the electron resides. The inner potential is defined by the amount of electrostatic work done to bring an electron from the vacuum at infinity to a location just inside the phase $i$ and, therefore, contains the contribution due to the work done by the electron when it crosses the liquid vacuum interface. An estimate of this work term is given by the calculated absolute potential of the reference electrode.[53] However, since we will be considering the difference in chemical potentials, this interfacial work term cancels out in most cases. This work contribution can, thus, be ignored without any loss of information. In this context, the inner potential for the metal is equal to the applied potential at the metal surface ($\varphi_M$). This follows from the assumption that the charge transfer resistance at the metal−monolayer interface due to the gold thiol bond ($R_{ct1}^{\text{monolayer}}$) is much smaller than the potential barrier at the monolayer−electrolyte interface ($R_{ct2}^{\text{monolayer}}$). In the case of the electrochemical potential of an electron at the interface between the monolayer and the electrolyte, the electron transfers between the bonding orbitals of the ion/neutral electrolyte species at the outer Helmholtz plane that can act as the electron donor or acceptor, and the LUMO of the functional group in the monolayer phase. Thus, the inner potential for the Stern layer, defined by the amount of electrostatic work done to bring an electron from infinity to a location just inside the inner Helmholtz plane, is given by $\varphi_{IHP} - \varphi_{OHP} + \varphi_{OHP} = \varphi_{IHP}$. Note that in defining a(n) (electro)chemical potential for an electron at the inner Helmholtz plane, we have assumed that a proper ensemble can be defined with respect to electrons at the inner Helmholtz plane that are transferred either from or to ionic/neutral electrolyte species at the outer Helmholtz plane that act as electron donors/acceptors. The existence of this ensemble of electrons at the inner Helmholtz plane is implied by the nature of the experimental system itself, where the measured current density is not from a countable number of electron transfer events but is, instead, averaged over a large population of self-assembled monolayer molecules ($\sim 10^{16}$ molecules). The identity of the electron-donating or -accepting ionic/neutral species that participate in the interface reaction is not required in the scope of discussions here and is elaborated on elsewhere.[33]

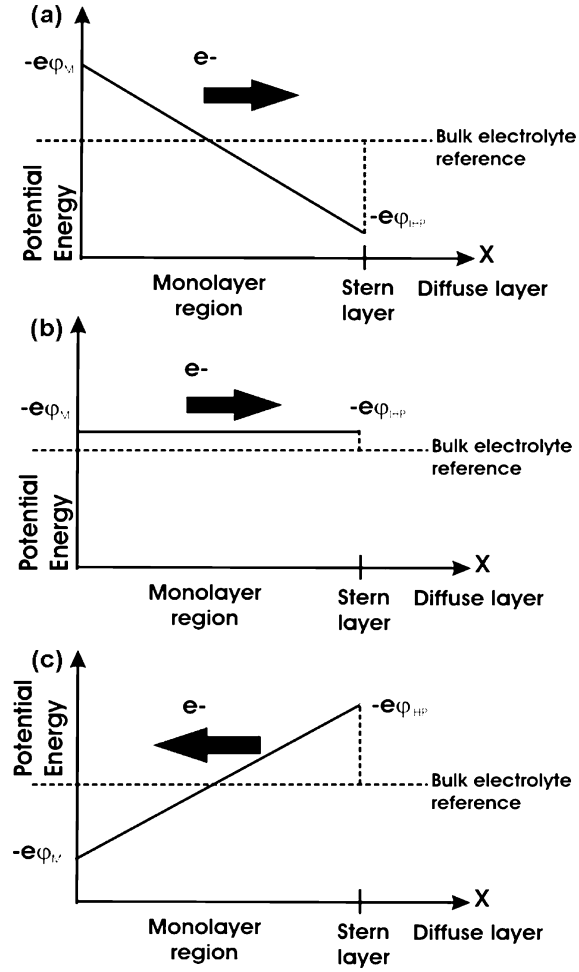


**Figure 7.** Schematic representation of the electrostatic potential energy profiles and the direction of electron flow (arrows) for (a) cathodic potentials, (b) the PZF, and (c) anodic potentials.

The application of a cathodic bias at the metal with respect to the bulk electrolyte solution results in a reduction current in which the applied bias increases the free energy of the electrons in the metallic phase, as seen from eq 28. Simultaneously, the applied bias also modifies the bending of the potential profile at the IHP by reducing the electrostatic energy of the electron at this location (Figure 7a). At some critical potential, the electrostatic potential at the metal equals the potential at the IHP (Figure 7b). Thus, the difference in the free energy of the electrons between the IHP and the metal is equal to the difference in the chemical potentials of the electrons between the two locations so that the electric field in the monolayer reduces to zero. At the PZF, the current in the monolayer is driven by the difference in chemical potentials only and, hence, is purely diffusive in nature.[45] In another paper, we show that for increasingly cathodic potentials, the current continues to exhibit this diffusion limited behavior.[33] Anodic potentials

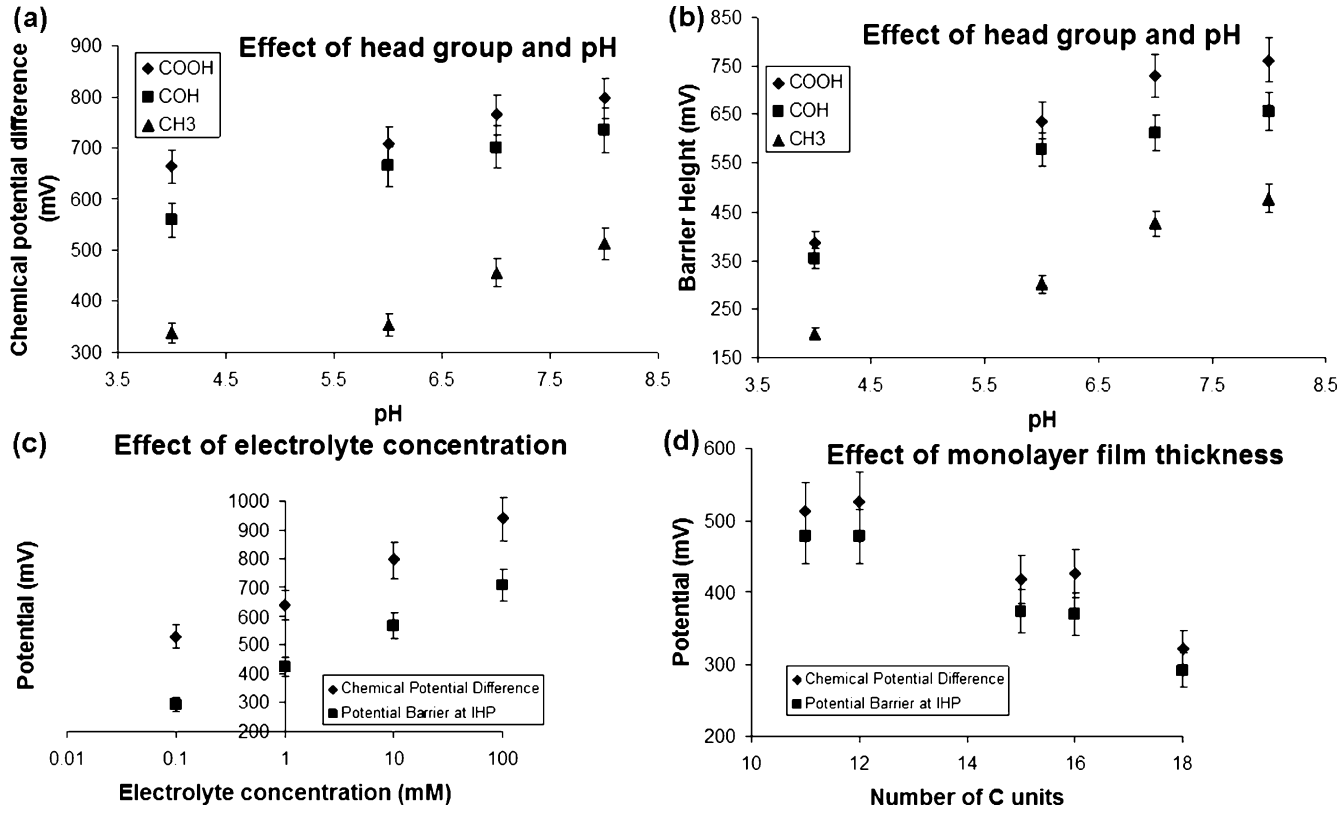


**Figure 8.** The effect of electrolyte pH and functional group on (a) the chemical potential difference between an electron in the metal and at the IHP and (b) the potential barrier height at the IHP. For these experiments, the monolayer film is 10 methylene units long, and the electrolyte is a 10 mM aqueous phosphate buffer. Also shown are the trends in the chemical potential difference and the potential barrier height due to varying (c) electrolyte concentration, and (d) monolayer film thickness. The monolayer film in part c is 1-mercaptodecanoic acid, and the electrolyte is an aqueous phosphate buffer at pH 4. For the experiments in part d, the monolayer has a methyl-terminated functional group, and the electrolyte is a 10 mM phosphate buffer solution at pH 8.

applied to the metal, on the other hand, result in a net oxidation current, decrease the free energy of the electrons in the metal, and increase the electrostatic energy of the electrons at the IHP (Figure 7c). At a specific value of equilibrium potential (Figure 6c), the electrochemical potential of the electrons in the metal equals the electrochemical potential of the electrons at the IHP. Thus, the net current density reduces to zero (Figure 6c), and the monolayer behaves as a perfect capacitor at this potential. At this equilibrium potential, the difference in chemical potentials of electrons at the metal and the IHP is obtained by equating the electrochemical potentials at the two locations, such that

$$\left(\mu_e^M - \mu_e^{IHP}\right)_{eq} = e(\phi_M - \phi_{IHP})_{eq} = eE_{eq}\beta \qquad (29)$$

where $E_{eq}$ is the value of the electric field at the equilibrium potential obtained by evaluating eq 6b at the equilibrium potential, and $\mu_e^{IHP}$ is the chemical potential of the electron at the IHP. Equation 29 also describes the thermodynamic properties of a specific monolayer−electrolyte interface and is similar to eq 27 because $\mu_e^M$ is the same for all gold−monolayer−electrolyte systems considered here. However, the description of the interface provided by eq 29 is in terms of the chemical potential referenced to the chemical potential of the underlying gold substrate at equilibrium conditions, as opposed to the description in eq 27, which is in terms of the potential at the IHP referenced to the bulk electrolyte solution. Note that the descriptions provided here implicitly assume that the impedance of the monolayer and the monolayer−electrolyte interface exceeds the impedance due to the diffuse layer and the solution resistance. This assumption is justified given that the impedance response does not display any Warburg-like characteristics that would suggest that mass transfer of the ion to the OHP is rate-limiting.[10] In addition, the real part of the system admittance ($Y_{sys}^{Re}$), calculated from eq 5a, is positive and significantly larger than the solution resistance for the entire range of the potential spectrum and in all the systems considered here.

**Built-In Electric Field and Equilibrium Chemical Potential Difference As Functions of Electrolyte and Monolayer Properties.** The chemical potential difference at equilibrium and the potential barrier at the IHP for the conditions of zero applied bias are shown in Figure 8a and b, respectively, as functions of electrolyte pH and the functional end groups. Both the equilibrium chemical potential difference and the potential barrier at the IHP indicate that an increase in the pH or electronegativity of the end group decreases the chemical potential of transported electrons at the IHP and makes the potential at the IHP more negative. The two results are consistent because an increasingly negative IHP potential presents a larger barrier for the electrons to cross over, which reduces the number of energy states available to electrons at the IHP and, hence, the chemical potential of the electrons at that location.[45] The hypothesis works in the limit that the electrons at the IHP can be treated as a classical gas with minimal self-interactions. In a separate paper, we demonstrate the applicability of this limit to the gold−monolayer−electrolyte systems investigated here.[33] Both the chemical potential difference and the potential barrier at the IHP also increase linearly with the logarithm of the bulk electrolyte concentration (Figure 8c). Note the linear dependence of the two parameters on the pH and the log of concentration, which we will elaborate on later. Figure 8d depicts the two

physicochemical parameters as functions of the number of carbon atoms that form the backbone of the monolayer film. Here, we define the number of carbon atoms as the total number of methylene moieties in the alkane backbone plus the methyl unit that makes up the functional group. From Figure 8d, it is evident that both thermodynamic properties of the monolayer−electrolyte interface (namely, the difference in free energy for the electrons between the metal and the IHP and the electrostatic potential energy barrier at that plane) decrease with increasing thickness of the monolayer phase. Therefore, the chemical potential of the methyl functional group at the monolayer−electrolyte interface increases and the corresponding electronegativity decreases with increasing thickness of the monolayer film. We hypothesize that the observed decrease in barrier height for thicker monolayer films is due to a decrease in the electrostatic repulsion forces acting at methyl surface sites as the distance between these sites and the metal surface is increased. The larger spacing between the metal surface and the methyl functional group of the alkane chain lowers the Coulombic repulsion between the electrons of the metal and the electrons at the methyl moiety, making the methyl functional groups more electropositive. The decrease in the chemical potential difference and the potential barrier with an increase in the number of carbon units in the monolayer film is not monotonic, and an oscillation in the values of these two parameters is evident in Figure 8d. From the literature, it is known that the $sp^3$ hybridized structure of the alkane backbone implies that the increase in the monolayer film thickness for an odd number of carbon units in the alkane backbone is 1.34 Å, whereas the corresponding thickness increase for an even number of carbon atoms is only 0.9 Å.[68] Thus, the chemical potential difference and potential barrier parameters display a small increase over and above the generally decreasing trend as the number of carbon moieties goes from odd to even.

The two physicochemical characteristics of the monolayer−electrolyte interface (namely, the built-in electric field and the equilibrium chemical potential difference) exist in the potential regime (Figures 6a and c) in which the response of the gold−monolayer−electrolyte system is predominantly capacitive (Figure 1a). Thus, the monolayer film primarily stores charge at the metal and Stern layer plane (Figure 3b) that confine the film on both sides, and a small amount of charge "leaks" through the organic film. The experimental system is analogous to a parallel plate capacitor sandwiching a thick dielectric between the plates that stores most of the charge pumped into the system and allows only a small amount of charge to leak between the plates. Any observed current density in the thick-dielectric, parallel plate capacitor system is limited by the rate of charge transport through the dielectric medium. Similarly, the rate-limiting process in a gold−monolayer−electrolyte system that has a capacitive response to the applied potential is, expectedly, the rate of charge transport within the monolayer structure. Therefore, the kinetics of the charge transfer process at the monolayer−electrolyte interface is faster than the rate of charge transport through the monolayer phase such that the monolayer−electrolyte interface reaction can be considered to be at quasi-equilibrium (i.e., $R_{ct2}^{monolayer} \ll R_{monolayer}$). This hypothesis is also supported by the deduction that the current density expressions for this potential regime obey specific mechanistic descriptions of charge transport.[33] Note that the kinetics of electron transfer at a monolayer−electrolyte interface in the absence of redox-active molecules might be significantly slower than the rate of charge transfer between an electroactive moiety and a solid electrode. However, the appropriate comparison here is between the faster electron transfer kinetics at the monolayer−electrolyte interface and the slower charge transport rate through the monolayer phase, which leads into our quasi-equilibrium hypothesis discussed above. As discussed before, the transport of ionic/neutral electrolyte reactants to the OHP is not rate-limiting, and so trace electroactive impurities in the electrolyte do not contribute significantly to the observed current flow. Since the electrons at the IHP and donor/acceptor levels of the electrolyte constituents at the OHP participating in the charge transfer process are in equilibrium with each other, and since the electrolyte species at the OHP are in equilibrium with the corresponding moieties in the bulk, as discussed before, equilibrium between the electrons at the IHP and in the bulk electrolyte solution can be safely assumed, yielding

$$\mu_e^{IHP} - e\phi_{IHP} = \mu_e^{bulk} \tag{30}$$

The notional (electro)chemical potential of an electron in the bulk electrolyte solution is given by $\mu_e^{bulk}$ in expression 30. Since the number density of free electrons in aqueous electrolytes is negligible,[71] this chemical potential term describes the donor or acceptor energy level of the ion/neutral electrolyte species in the bulk electrolyte that interacts with the metal phase via a charge transfer process. Substituting eq 30 into eq 29 gives

$$(\mu_e^{M} - \mu_e^{bulk} - e\phi_{IHP})_{eq} = eE_{eq}\beta \tag{32}$$

Thus, if the equilibrium potential for the gold−monolayer−electrolyte system lies in the range of potentials where current is charge-transport-limited, the experimentally determined quantity $E_{eq}$ should contain information not just about the monolayer−electrolyte interface, but also about the bulk electrolyte solution. Similarly, in these potential regimes, $E_{bi}$ (and hence, $\varphi_{IHP}$) should carry information about the donor or acceptor level of those electrolyte constituents in the bulk electrolyte that participate in the charge transfer process.

The donor/acceptor energy levels in the electrolyte constituents that exchange charge with the metal phase follow a Gaussian-modified Boltzmann-type distribution when the electrolyte solution is dilute, where collisions of the electrolyte constituents with solvent molecules account for the Gaussian spread in the ground-state energy of the energy levels of the electrolyte constituents.[10,71] Thus, the notional (electro)chemical potential of the electron in the bulk electrolyte solution introduced above has been approximated by the mean vibrational ground-state energy of the solvent−electrolyte constituent bond in solution.[71] Since the vibrational energies of these bonds in a solvated ion complex have a Boltzmann distribution over a large energy range, the (electro)chemical potential of an electron in solution can be treated classically.[45] Thus, the bulk electrolyte chemical potential of an electron is dependent on the concentration ($c$) of the electron carrying species ($OH^-$, $H_2PO_4^-$, $HPO_4^{2-}$); that is,

$$|\mu_e^{bulk}| \propto \ln[c] \tag{33a}$$

and

$$|\mu_e^{bulk}| \propto 14 - \mathrm{pH} \tag{33b}$$

Gurney[72] demonstrated that as the concentration of the anion or the hydroxyl radical increases, the notional chemical potential of electrons in the bulk electrolyte solution ($\mu_e^{bulk}$) decreases. This point is well-illustrated by the monotonic linear increase in $E_{eq}$ and $E_{bi}$ with pH and concentration in Figure 8a−c. The linear dependence of $E_{eq}$ and $E_{bi}$ on bulk electrolyte conditions supports our initial assumption about quasi-equilibrium condi-

tions for the monolayer−electrolyte interface reaction. However, $E_{eq}$ and $E_{bi}$ also decrease with the monolayer film thickness (Figure 8d), although bulk electrolyte properties are maintained for each monolayer film. Thus, for anodic potentials in which the response is capacitive, sizable variations in bulk electrolyte properties tend to mask the effect that any corresponding change at the monolayer−electrolyte interface might have on observable parameters, such as $E_{eq}$ and $E_{bi}$. However, in cases that the electrolyte properties are invariant, variations in these parameters can be attributed to conditions specific to a particular monolayer−electrolyte interface.

The electric field in the monolayer and the net current density of a specific gold−monolayer−electrolyte system are used to derive the thermodynamic properties, $(\mu_e^M - \mu_e^{IHP})_{eq}$ and $\varphi_{IHP}$, described above. The calculation of the electric field or the net current density from eqs 6a and 6b involves no assumption about the presence or absence of pinholes in the film through which ionic or neutral charge exchanging electrolyte constituents can penetrate. However, the physical interpretation of $E_{bi}$ and $E_{eq}$ is clearly dependent on the model of the charge transport process in the monolayer film. The barrier to charge transfer exists at the gold−electrolyte interface within the pinhole structure for a monolayer film with large pinholes (Figure 1c). For this case, $E_{bi}$ is then the zero-bias electrostatic field in the pinhole structure, and $E_{eq}$ would describe the chemical potential difference between the energy levels of the electrolyte constituents at the location of the functional group and the energy level of the corresponding electrolyte constituent at the gold−electrolyte interface. If the pinhole size is large enough to facilitate the penetration of electrolyte constituents that participate in charge exchange with the gold phase, the effect of the functional end group on the barrier height should be weak. Even if the functional groups were to exert a significant electrostatic field at the entrance of the pinhole, the more electronegative end groups would lower the transport barrier because they would inhibit penetration of anion/hydroxyl ions within the pinholes for anodic potentials. The results described in the previous section, however, indicate that the interface barrier is larger for more electronegative end groups, suggesting that the transport of charge carriers through pinhole defects in the monolayer structure does not contribute significantly to the observed current density.

The existence of quasi-equilibrium conditions between the charge exchange interface and the bulk electrolyte solution, as demonstrated in Figure 8a−c also disproves the possibility that charge conduction in the monolayer phase is due to ion penetration in the monolayer film. For the case of large pinholes, we have seen that the only charge transfer barrier exists at the gold−electrolyte interface and the charge transport barrier characterizes the impedance to the motion of charge carriers in the pinhole (Figure 2c). Thus, for the anodic potential regime, in which charge transport is rate-limiting, the gold−electrolyte interface cannot be at equilibrium with the bulk electrolyte solution, since the charge transfer barrier at the gold−electrolyte interface is spatially decoupled from the electrolyte phase by the monolayer film that kinetically limits the charge flow process. However, as mentioned before, the linear dependence of the monolayer−electrolyte parameters ($E_{eq}$, $E_{bi}$) on bulk electrolyte conditions (Figur 8a−c) indicates that since the charge transfer interface and the bulk electrolyte solution are at quasi-equilibrium with each other, hence, they must be spatially coupled to each other. Thus, only if the charge transfer barrier is located at the monolayer−electrolyte interface can there be equilibrium between the charge transfer barrier and the bulk electrolyte solution. By this reasoning, we can rule out the contribution of charge carriers through pinholes to the observed current density.

## Conclusion

We have presented here a derivation of a mathematical model to better understand the charge transfer characteristics of a gold−monolayer−electrolyte system for the specific case when the electrolyte does not contain any redox-active ions. The method described here utilizes a constitutive charge transport equation to calculate the free charge density and electric field within the monolayer film from experimental low-frequency impedance data. In applying the mechanistic description of charge transport to impedance data, we do not rely on a phenomenological linear circuit analysis to explain the nonlinear current−potential behavior of gold−monolayer−electrolyte systems. The application of the charge transport equation to describe the charge flux through these electrochemical systems also does not require a detailed explanation of the kinetics of the charge transfer that occurs at the monolayer−electrolyte interface between the monolayer functional group and the donor/acceptor electrolyte constituents. A scaling analysis to calculate charge mobility and diffusivity of charge within the monolayer is also outlined. The results for average monolayer conductivity in the presence of a weak monolayer electric field, calculated using the estimated mobility value, agrees well with published data. The agreement between the average conductivity of the monolayer film and the reported low-field conductivity for organic thin films indicates that the primary mechanism of charge transport is, indeed, through the alkane backbone structure of the monolayer phase and not through pinhole defects in the monolayer film.

The variation of the electric field with the applied potential yields two physicochemical characteristics: namely, the built-in electric field ($E_{bi}$) and the chemical potential difference for an electron between the metal and the IHP at equilibrium conditions $(\mu_e^M - \mu_e^{IHP})_{eq}$, that enable the description of the monolayer−electrolyte interface in terms of the bulk electrolyte properties. The equilibrium that results between the IHP and the bulk electrolyte occurs for potentials that are more anodic than the PZF. Within this potential regime, the thin-film-modified electrode can conceivably act as a concentration or pH sensor that can evaluate bulk electrolyte properties. However, the two characteristics reflect properties specific to the monolayer−electrolyte interface for experimental systems with invariant bulk electrolyte properties. In separate work[33] we investigate the charge transport within the monolayer film and the charge transfer reactions at the monolayer−electrolyte interface using the values of free charge density and monolayer electric field, which are calculated from the equations developed here. Furthermore, we are presently working on using the methodology developed in this paper to estimate surface charge densities at the monolayer−electrolyte interface for these thin film structures.

**Acknowledgment.** This work was performed within Nano-CEMMS; UIUC's Nano-Science and Engineering Center (NSEC), supported by the National Science Foundation under Award no. DMI-0328162. XPS was carried out in the Frederick Seitz Materials Research Laboratory Central Facilities, University of Illinois, supported in part by the U.S. DOE under Grants DE-FG02-07ER46453 and DE-FG02-07ER46471. The authors also acknowledge Dr. Rick Haasch for assistance with the XPS measurements.

## References and Notes


(1) Bigelow, W. C.; Pickett, D. L.; Zisman, W. A. *J. Colloid Interface Sci.* **1946**, *1*, 513.

(2) Nuzzo, R. G.; Allara, D. L. *J. Am. Chem. Soc.* **1983**, *105*, 4481.

(3) Nuzzo, R. G.; Zegarski, B. R.; Dubois, L. H. *J. Am. Chem. Soc.* **1987**, *109*, 733.

(4) Nuzzo, R. G.; Dubois, L. H.; Allara, D. L. *J. Am. Chem. Soc.* **1990**, *112*, 558.

(5) Chidsey, C. E. *Science* **1991**, *251*, 919.

(6) Bard, A. J.; Abruna, H. J.; Chidsey, C. E.; Faulkner, L. R.; Feldberg, S. W.; Itaya, K.; Majda, M.; Melroy, O.; Murray, R. W.; Soriaga, M. P.; White, H. S. *J. Phys. Chem.* **1993**, *97*, 7147.

(7) Finklea, H. O.; Hanshew, D. D. *J. Am. Chem. Soc.* **1991**, *114*, 3173–3181.

(8) Finklea, H. O.; Ravenscroft, M. E.; Snider, D. A. *Langmuir* **1993**, *9*, 223.

(9) Acevedo, D.; Abruna, H. D. *J. Phys. Chem.* **1991**, *95*, 9590.

(10) Bard, A. J.; Faulkner, L. R., *Electrochemical Methods: Fundamentals and Applications.* John Wiley & Sons, Inc.: New York, 2001.

(11) Miller, C.; Cuendet, P.; Gratzel, M. *J. Phys. Chem.* **1991**, *95*, 877.

(12) Becka, A.; Miller, C. J. *J. Phys. Chem.* **1992**, *96*, 2657.

(13) Chidsey, C. E.; Loiacono, D. N. *Langmuir* **1990**, *6*, 682.

(14) Smalley, J. F.; Finklea, H. O.; Chidsey, C. E. D.; Linford, M. R.; Creager, S. E.; Ferraris, J. P.; Chalfant, K.; Zawodzinsk, T.; Feldberg, S. W.; Newton, M. D. *J. Am. Chem. Soc.* **2003**, *125*, 2004.

(15) Finklea, H. O. *J. Phys. Chem. B* **2001**, *105*, 8685.

(16) Lyons, M. E. G. *Sensors* **2002**, *2*, 314.

(17) Newton, M. D.; Smalley, J. F. *Phys. Chem. Chem. Phys.* **2007**, *9*, 555.

(18) Liu, B.; Bard, A. J.; Mirkin, M. V.; Creager, S. E. *J. Am. Chem. Soc.* **2004**, *126*, 1485.

(19) Finklea, H. O.; Hanshew, D. D. *J. Am. Chem. Soc.* **1991**, *114*, 3173.

(20) Porter, M. D.; Bright, T. B.; Allara, D. L.; Chidsey, C. E. *J. Am. Chem. Soc.* **1987**, *109*, 3559.

(21) Nahir, T. M.; Bowden, E. F. *J. Electroanal. Chem.* **1996**, *410*, 9.

(22) Adams, D. M.; Brus, L.; Chidsey, C. E.; Creager, S. E.; Creutz, C.; Kagan, C. R.; Kamat, P. V.; Lieberman, M.; Lindsay, S.; Marcus, R. A.; Metzger, R. M.; Michel-Beyerle, M. E.; Miller, J. R.; Newton, M. D.; Rolison, D. R.; Sankey, O.; Schanze, K. S.; Yardley, J.; Zhu, X. *J. Phys. Chem. B* **2003**, *107*, 6668.

(23) Bain, C. D.; Whitesides, G. M. *Langmuir* **1989**, *5*, 1370.

(24) Dubois, L. H.; Zegarski, B. R.; Nuzzo, R. G. *J. Am. Chem. Soc.* **1990**, *112*, 570.

(25) Ulman, A., *An Introduction to Ultrathin Organic Thin Films From Langmuir-Blodgett to Self Assembly*; Academic Press: San Diego, 1991.

(26) Pallandre, A.; de Lambert, B.; Attia, R.; Jonas, A. M.; Viovy, J. L. *Electrophoresis* **2006**, *27*, 584.

(27) Andreu, R.; Fawcett, W. R. *J. Phys. Chem.* **1994**, *98*, 12753.

(28) Smith, C. P.; White, H. S. *Anal. Chem.* **1992**, *64*, 2398.

(29) Smith, C. P.; White, H. S. *Langmuir* **1993**, *9*, 1.

(30) Schweiss, R.; Werner, C.; Knoll, W. *J. Electroanal. Chem.* **2003**, *540*, 145.

(31) Boubour, E.; Lennox, R. B. *J. Phys. Chem. B* **2000**, *104*, 9004.

(32) Boubour, E.; Lennox, R. B. *Langmuir* **2000**, *16*, 4222.

(33) Gupta, C.; Shannon, M. A.; Kenis, P. J. A. *J. Phys. Chem. C* **2008**, *113*, 4687.

(34) Komura, T.; Yamaguchi, T.; Shimatani, H.; Okushio, R. *Electrochim. Acta* **2004**, *49*, 597.

(35) Creager, S. E.; Wooster, T. T. *Anal. Chem.* **1998**, *70*, 4257.

(36) Komura, T.; Yamaguchi, T.; Takahashi, K.; Terasawa, H. *J. Electroanal. Chem.* **2000**, *481*, 183.

(37) Molinero, V.; Calvo, E. J. *J. Electroanal. Chem.* **1998**, *445*, 17.

(38) Boubour, E.; Lennox, R. B. *Langmuir* **2000**, *16*, 7464.

(39) Burgess, I.; Seivewright, B.; Lennox, R. B. *Langmuir* **2006**, *22*, 4420.

(40) Dubois, L. H.; Nuzzo, R. G. *Annu. Rev. Phys. Chem.* **1992**, *43*, 437.

(41) Love, J. C.; Estroff, L. A.; Kriebel, J. K.; Nuzzo, R. G.; Whitesides, G. M. *Chem. Rev.* **2005**, *105*, 1103.

(42) Sze, S. M.; Kwok, K. N. *Physics of Semiconductor Devices*; Wiley-Interscience: New York, 2006; p 815.

(43) Slowinski, K.; Chamberlain, R. V.; Miller, C. J.; Majda, M. *J. Am. Chem. Soc.* **1997**, *119*, 11910.

(44) Hill, R. M. *Philios. Mag.* **1971**, *23*, 59.

(45) Kittel, C.; Kroemer, H., *Thermal Physics*, 2nd ed.; W. H. Freeman: New York, 1980; p 496.

(46) Sun, Q.; Selloni, A. *J. Phys. Chem. A* **2006**, *110*, 11396.

(47) Campbell, I. H.; Rubin, S.; Zawodzinski, T. A.; Kress, J. D.; Martin, R. L.; Smith, D. L.; Barashkov, N. N.; Ferraris, J. P. *Phys. Rev. B* **1996**, *54*, 14321.

(48) Simmons, J. G. *J. Appl. Phys.* **1964**, *35*, 2472.

(49) Kroger, F. A.; Diemer, G.; Klasens, H. A. *Phys. Rev.* **1956**, *103*, 279.

(50) *CRC Handbook of Chemistry and Physics*, 88th ed.; CRC Press/Taylor and Francis: Boca Raton, 2008.

(51) Jackson, J. D., *Classical Electrodynamics*; John Wiley: New York, 1998; p 809.

(52) Grahame, D. C. *Chem. Rev.* **1947**, *41*, 441.

(53) Bockris, J. O. M.; Conway, B. E.; Yeager, E. *Comprehensive Treatise of Electrochemistry: The Double Layer*; Plenum Press: New York, 1980; Vol. 1, p 453.

(54) Levine, S.; Mingins, J.; Bell, G. M. *J. Electroanal. Chem.* **1967**, *13*, 280.

(55) Levine, S. *J. Colloid Interface Sci.* **1971**, *37*, 619.

(56) Barlow, C. A.; MacDonald, J. R. *J. Chem. Phys.* **1964**, *40*, 1535.

(57) Boulas, C.; Davidovits, J. V.; Rondelez, F.; Vuillaume, D. *Phys. Rev. Lett.* **1996**, *76*, 4797.

(58) Rampi, M. A.; Schueller, O. J. A.; Whitesides, G. M. *Appl. Phys. Lett.* **1998**, *72*, 1781.

(59) Laibinis, P. E.; Whitesides, G. M.; Allara, D. L.; Tao, Y.; Parikh, A. N.; Nuzzo, R. G. *J. Am. Chem. Soc.* **1991**, *113*, 7152.

(60) Nuzzo, R. G.; Dubois, L. H.; Allara, D. L. *J. Am. Chem. Soc.* **1990**, *112*, 558.

(61) Kreyszig, E., *Advanced Engineering Mathematics*, 5th ed.; John Wiley & Sons: New York, 1983; p 988.

(62) Everett, R. W.; Fritsch-Faules, I. *Anal. Chim. Acta* **1995**, *307*, 253.

(63) Rodriguez, J. F.; Mebrahtu, T.; Soriaga, M. P. *J. Electroanal. Chem.* **1987**, *233*, 283.

(64) Watanabe, T.; Gerischer, H. *J. Electroanal. Chem.* **1981**, *117*, 185.

(65) Oesch, U.; Janata, J. *Electrochim. Acta* **1983**, *28*, 1237.

(66) Walczak, M. M.; Popenoe, D. D.; Deinhammer, R. S.; Lamp, B. D.; Chung, C.; Porter, M. D. *Langmuir* **1991**, *7*, 2687.

(67) Zhong, C.-J.; Zak, J.; Porter, M. D. *J. Electroanal. Chem.* **1997**, *421*, 9.

(68) Smalley, J. F.; Feldberg, S. W.; Chidsey, C. E.; Linford, M. R.; Newton, M. D.; Liu, Y. *J. Phys. Chem.* **1995**, *99*, 13141.

(69) Mott, N. F. *Proc. R. Soc. A* **1939**, *171*, 27.

(70) Brillson, L. J. *Surf. Sci. Rep.* **1982**, *2*, 123.

(71) Bockris, J. O. M.; Reddy, A. K. N.; Gamboa-Aldeco, M., *Modern Electrochemistry 2A: Fundamentals of Electrodics*; 2nd ed.; Plenum: New York, 2000; Vol. 2A, pp 771−1529.

(72) Gurney, R. W. *Proc. R. Soc. A* **1931**, *134*, 137.


JP900918U